

# An introduction to Cosmic Rays and Gamma-Ray Bursts, and to their simple understanding

Alvaro De Rújula  
*CERN & Boston University*

## Abstract

I review the subjects of non-solar cosmic rays (CRs) and long-duration gamma-ray bursts (GRBs). Of the various interpretations of these phenomena, the one best supported by the data is the following. Accreting compact objects, such as black holes, are seen to emit relativistic puffs of plasma: ‘cannonballs’ (CBs). The inner domain of a rotating star whose core has collapsed resembles such an accreting system. This suggests that core-collapse supernovae (SNe) emit CBs, as SN1987A did. The fate of a CB as it exits a SN and travels in space can be studied as a function of the CB’s mass and energy, and of ‘ambient’ properties: the encountered matter- and light- distributions, the composition of the former, and the location of intelligent observers. The latter may conclude that the interactions of CBs with ambient matter and light generate CRs and GRBs, all of whose properties can be described by this ‘CB model’ with few parameters and simple physics. GRB data are still being taken in unscrutinized domains of energy and timing. They agree accurately with the model’s predictions. CR data are centenary. Their precision will improve, but new striking predictions are unlikely. Yet, a one-free-parameter description of all CR data works very well. This is a bit as if one discovered QED today and only needed to fit  $\alpha$ .

## 1 Introduction

This is a version of an introductory talk to high-energy physicists. Cosmic rays (CRs) were the first item in their field, and will remain the energy record-breakers for the foreseeable future. I shall argue that nothing ‘besides the standard model’ is required to understand CRs of any energy, subtracting from their interest. ‘Long’ gamma-ray bursts (GRBs) are flashes of mainly sub-MeV photons, originating in supernova (SN) explosions. The  $\gamma$ -rays are highly collimated. Hence, GRBs are not the publicized ‘highest-energy explosions after the big bang’, but more modest torches occasionally pointing to the observer. GRBs are of interest because their understanding is intimately related to that of CRs. It might have been more precise to say ‘my understanding’ of GRBs and CRs, for the work of my coauthors and I is viewed as unorthodox.

What a start! I have already admitted that our stance is not trendy and that the subject is of no post-standard interest. But our claims are based on

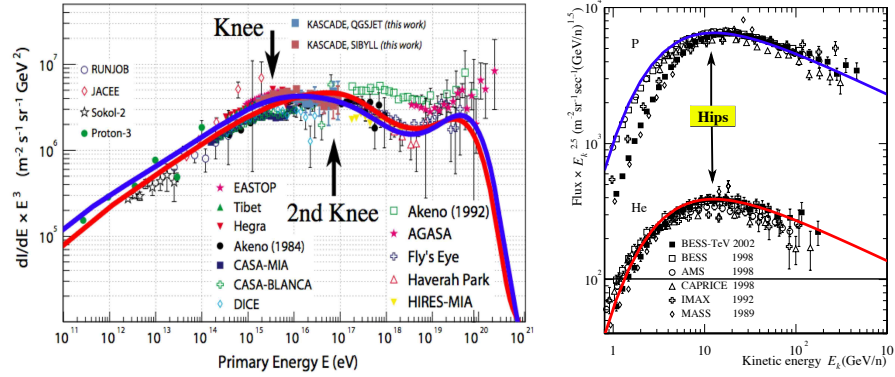


Figure 1: **Left (a)** The weighed all-particle CR spectrum  $E^3 dF/dE$ . Some of the high-energy data disagree with others. **Right (b)** The low-energy H and He flux versus the kinetic energy per nucleon, multiplied by  $E_{\text{kin}}^{2.5}$ . In (a) the lines are two extreme CB-model predictions. In (b) both lines are predictions. The data coincide best with the prediction at solar minimum. The normalizations, shown here to coincide with the data, are predicted to within a factor of  $\sim 3$ .

clear hypothesis, which may be proven wrong, and very basic physics, which is precise enough, very pretty, understandable to undergraduates, and successful.

The information about GRBs and CRs is overwhelming. GRBs are known since the late 60's and CRs since 1912. Surprisingly, no theories have arisen that are both accepted ('standard') and acceptable (transparent, predictive and successful). I cannot refer to a representative subset of the  $\sim 70+70$  kilopapers on CRs and GRBs. For reviews of the standard views on CRs, see e.g. Hillas <sup>1)</sup> or Hoerandel <sup>2)</sup>. For the accepted 'fireball' model of GRBs see e.g. Meszaros <sup>3)</sup> or Piran <sup>4)</sup>. Fewer self-citations and many more references, particularly to data, appear in DDD02 <sup>5)</sup>, DDD03 <sup>6)</sup>, DD04 <sup>7)</sup> and DD06 <sup>8)</sup>.

## 2 Most of what you may want to recall about Cosmic Rays

In CR physics 'all-particle' refers to nuclei: all charged CRs but electrons. The CR spectra being fairly featureless, it is customary to weigh them with powers of energy, to over-emphasize their features. The  $E^3 dF/dE$  all-particle spectrum is shown in fig. 1a, not updated for recent data at the high-energy tail. At less than TeV energies the CR flux is larger than  $1 \text{ m}^{-2} \text{ s}^{-1} \text{ sr}^{-1}$  and it is possible to measure the charge  $Z$  and mass number  $A$  of individual particles with, e.g., a magnetic spectrometer in a balloon, or in orbit. Some low-energy results for H and He are shown in fig. 1b. They vary with solar activity.

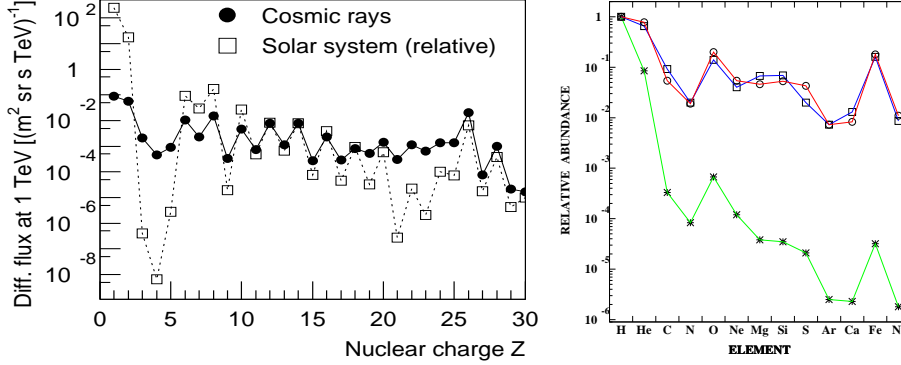


Figure 2: The CR fluxes at 1 TeV and the relative abundances in the ISM. **Left (a)** Fluxes of elements up to Z and abundances in the solar ISM. **Right (b)** Solar ISM abundances (stars), CR fluxes (squares) of the primary CRs, and the corresponding CB-model predictions (circles), all normalized to H.

The CR fluxes of the lightest 30 elements at  $E=1$  TeV (of a nucleus, not per-nucleon) are shown in fig. 2a, and compared with the relative abundances in the interstellar medium (ISM) of the solar neighbourhood. Elements such as Li, Be and B are relatively enhanced in the CRs, they result from collisional fragmentation of heavier and abundant ‘primaries’ such as C, N and O. Otherwise, the solar-ISM and CR  $Z$ -distributions are akin, but for H and He. In fig. 2b the abundances relative to H of the CR primary elements up to Ni ( $Z=28$ ) are plotted as blue squares. The stars are solar ISM abundances. CR positrons and antiprotons attract attention as putative dark matter products, but it is nearly impossible to prove that their fluxes are not entirely secondary.

The Galaxy has a complex magnetic-field structure with  $B_G = \mathcal{O}(1 \mu\text{G})$  and coherent domains ranging in size up to  $\sim 1$  kpc,  $\sim 1/8$  of our distance to the Galactic center. In such a field, a nucleus of  $E \simeq p > Z (3 \times 10^9)$  GeV would hardly be deflected. For  $Z=1$ , this energy happens to be the ‘ankle’ energy, at which the flux of fig. 1 bends up. CRs originating within the Galaxy and having  $E > E_{\text{ankle}}$  would escape practically unhindered. The CR flux does not bend *down* at that energy, thus the generally agreed conclusion that CRs above the ankle are mainly extragalactic. CRs of Galactic origin and  $E < E_{\text{ankle}}$  are ‘confined’, implying that their observed and source fluxes obey:

$$F_o \propto \tau_{\text{conf}} F_s, \quad \tau_{\text{conf}} \propto (Z/p)^{\beta_{\text{conf}}}, \quad \beta_{\text{conf}} \sim 0.6 \pm 0.1, \quad (1)$$

with  $\tau_{\text{conf}}$  a ‘confinement time’, deduced from the study of stable and unstable CRs and their fragments.

At  $E=10^6$ - $10^8$  GeV the all-particle spectrum of fig. 1a bends in one or

two ‘knees’. The knee flux is too small to measure directly its energy and composition, which are inferred from the properties of the CR shower of hadrons,  $\gamma$ ’s,  $e$ ’s and  $\mu$ ’s, initiated by the CR in the upper atmosphere. The results for H, He and Fe are shown in fig. 3. Note that even the same data leads to incompatible results, depending on the Monte-Carlo program used to analyze the showers. But the spectra of the various elements seem to have ‘knees’ which scale roughly with  $A$  or  $Z$ , the data not been good enough to distinguish.

The high- $E$  end of the  $E^3$ -weighed CR spectrum is shown in fig. 4a. These data and the more recent ones of Hires and Auger, clearly show a cutoff, predicted by Greisen, Zatsepin and Kuzmin (GZK) as the result of the inevitable interactions of extragalactic CR protons with the microwave background radiation. The reactions  $p + \gamma \rightarrow n + \pi^+$ ;  $p + \pi^0$  cut off the flux at  $E > E_{\text{GZK}} \sim A \times 10^{11}$  GeV, from distances larger than tens of Mpc. Similarly, extragalactic nuclei of  $E > 10^9$  GeV are efficiently photo-dissociated in the cosmic infrared radiation, the corresponding CR flux should not contain many.

At very high energies, rough measures of the CR  $A$ -distribution are extracted from the ‘depth of shower maximum’,  $X$ , the number of grams/cm<sup>2</sup> of atmosphere travelled by a CR shower before its  $e^\pm/\gamma$  constituency reaches a maximum. At a fixed energy,  $X$  decreases with  $A$ , since a nucleus is an easily broken bag of nucleons of energy  $\sim E/A$ . As in fig. 4b, the data are often presented as  $\langle \ln[A](E) \rangle$ , which approximately satisfies  $X(A) \sim X(1) - x \ln[A]$ , with  $x \sim 37$  grams/cm<sup>2</sup> the radiation length in air.

If CRs are chiefly Galactic in origin, their accelerators must compensate for the escape of CRs from the Galaxy, to sustain the observed CR flux: it is known from meteorite records that the flux has been steady for the past few Giga-years. The Milky Way’s luminosity in CRs must therefore satisfy:

$$L_{\text{CR}} = \frac{4\pi}{c} \int \frac{1}{\tau_{\text{conf}}} E \frac{dF_o}{dE} dE dV \sim 1.5 \times 10^{41} \text{ erg s}^{-1}, \quad (2)$$

where  $V$  is a CR-confinement volume. The quoted standard estimate of  $L_{\text{CR}}$  is very model-dependent <sup>10)</sup>.

### 3 More than you ever wanted to know about Gamma-Ray Bursts

Two  $\gamma$ -ray count rates of GRBs, peaking at  $dN/dt = \mathcal{O}(10^4) \text{ s}^{-1}$ , are shown in fig. 5. The typical energy of the  $\gamma$ -ray of GBBs is  $\sim 250$  keV. The total ‘*isotropic equivalent*’ energy of a source of such photons at a typical redshift,  $z = \mathcal{O}(1)$ , is  $E_{\gamma}^{\text{iso}} \sim 10^{53}$  erg, similar to the available energy in a core-collapse SN explosion, i.e. half of the binding energy of a solar-mass neutron star, maybe a bit more for a black-hole remnant. It is hard to imagine a process with  $> 1\%$  efficiency for  $\gamma$ -ray production. Since GRBs are observed to be made by SNe, either the parent stars are amazingly special, or the  $\gamma$ -rays are narrowly beamed.

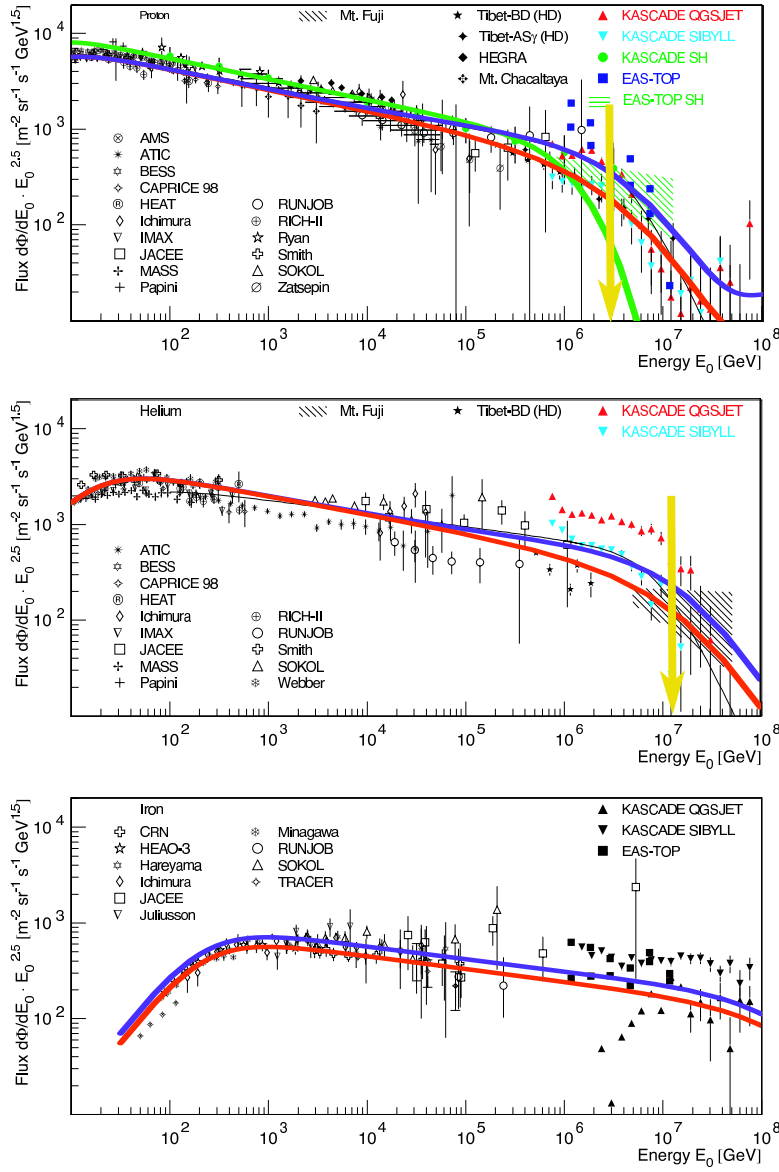


Figure 3:  $E^{2.5} dF/dE$  CR spectra in the ‘knee’ region. Top: protons; middle:  $\alpha$  particles; bottom: iron nuclei. The data ensemble was kindly provided by K.H. Kampert. The CB-model predictions are explained in the text. Notice the Fe ‘hip’, occurring at the same  $\gamma$  as the H, He hips of fig. 1b.

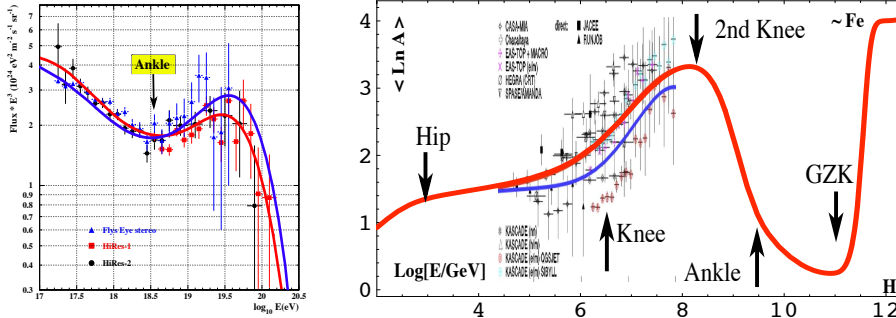


Figure 4: **Left (a)** The  $E^3$ -weighted CR flux at the highest observed energies. The data are not the oldest, nor the most recent, but show the currently observed trend. **Right (b)** The CR mean of the Neperian log of  $A$ , versus energy. In (a) the lines are two extreme CB-model predictions. The normalizations below and above the ankle, shown here to coincide with the data, are separately predicted to within a factor of  $\sim 3$ . In (b) the lines are as in (a).

The total-duration distribution of the  $\gamma$ -rays of GRBs has two peaks, with a trough at  $\sim 2$ s dividing (by definition) two distinct types. ‘Long’ GRBs are more common and better measured than short ones; one is more confident discussing mainly the former, as I shall. The long GRB light curves of fig. 5 are not atypical. The ‘pulses’ of a given GRB vary in intensity, but have similar widths, a fairly universal exponential rise, and a power decay  $\propto t^{-a}$ ,  $a \sim 2$ . The number of ‘clear pulses’ averages to  $\sim 5$ , it may reach  $\sim 12$ . The pulse-to-pulse delays are random, extending from  $\mathcal{O}(1\text{s})$  to  $\mathcal{O}(10^2\text{s})$ . Put all the above in a random-generator and, concerning long GRBs, ‘you have seen them all’.

GRBs are not often seen more than once a day, they are baptized with their observation date. GRBs 980425 and 030329, shown in fig. 5, originated at  $z = 0.0085$  (the record smallest) and 0.168, respectively. How are the redshifts known? GRBs have “afterglows” (AGs): they are observable in radio to X-rays for months after their  $\gamma$ -ray signal peters out. The AG of GRB 030329 in the ‘R-band’ (a red-light interval) and radio is shown in fig. 6a-c. Once the object is seen in optical or radio, its direction can be determined with much greater precision than via  $\gamma$  rays. Very often the source is localized within a galaxy, whose lines can be measured to determine  $z$  (in some cases a lower limit on  $z$  is deduced from absorption lines in intervening material).

GRB 980425 was ‘associated’ with a supernova called SN1998bw: within directional errors and within a timing uncertainty of  $\sim 1$  day, they coincided. The luminosity of a 1998bw-like SN peaks at  $\sim 15(1+z)$  days. The SN light competes at that time and frequency with the AG of its GRB, and it is not

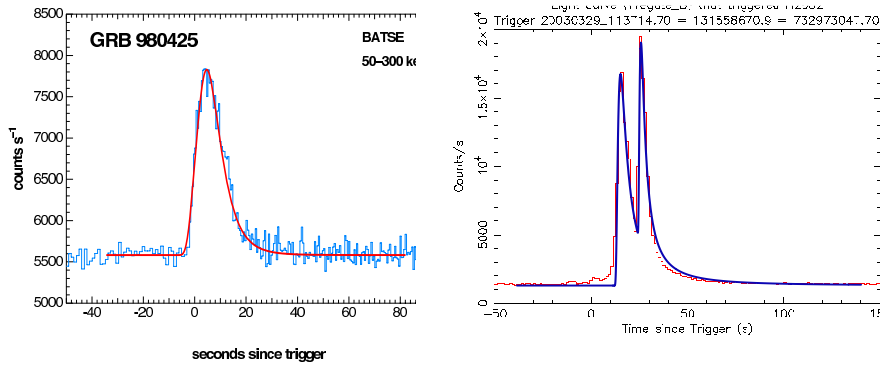


Figure 5: The  $\gamma$ -ray count-rate light curves of GRB 980425 (a: left) and GRB 030329 (b: right). In the CB model, each pulse corresponds to one cannonball. The single pulse in (a) and the two pulses in (b) are fit with Eq. 4.

always easily detectable. If one has a predictive theory of AGs, one may test whether GRBs are associated with ‘standard torch’ SNe, akin to SN1998bw, ‘transported’ to the GRBs’ redshifts. The test was already conclusive (to us) in 2001<sup>5)</sup>. One could even foretell *the date* in which a GRB’s SN would be discovered. For example, GRB 030329 was so ‘very near’ at  $z=0.168$ , that one could not resist posting such a daring prediction<sup>11)</sup> during the first few days of AG observations. The prediction and the subsequent SN signal are shown in fig. 6a,b. The spectrum of this SN was very well measured and seen to coincide snugly with that of SN1998bw, and this is why the SN/GRB association ceased to be doubted: *long GRBs are made by core-collapse SNe*.

Astrophysicists classify SNe in Types, mainly depending on the composition of their ejecta. Within very limited statistics the SNe associated with GRBs are of Type Ib/c. These constitute some 15% of core-collapse SNe, the fascinating ones which beget neutrinos, neutron stars and presumably black holes. Type Ia SNe are probably mere explosions of accreting white dwarfs, but they are very luminous, and of cosmological standard-candle fame.

GRBs have many ‘typical’ properties. Their spherical-equivalent number of  $\gamma$ -rays is  $\sim 10^{59}$ . Their spectrum at fixed  $t$  is very well approximated by:

$$\left. \frac{dN}{dE} \right|_t \propto \left[ \frac{T(t)}{E} \right]^\alpha e^{-E/T(t)} + b \left[ 1 - e^{-E/T(t)} \right] \left[ \frac{T(t)}{E} \right]^\beta \quad (3)$$

with  $b \sim 1$ ,  $\alpha \sim 1$ ,  $\beta \sim 2.1$ . Early in the evolution of a pulse, the ‘peak energy’ (characterizing the photons carrying most of the GRB’s energy) is  $E_p \sim T[0] \sim$

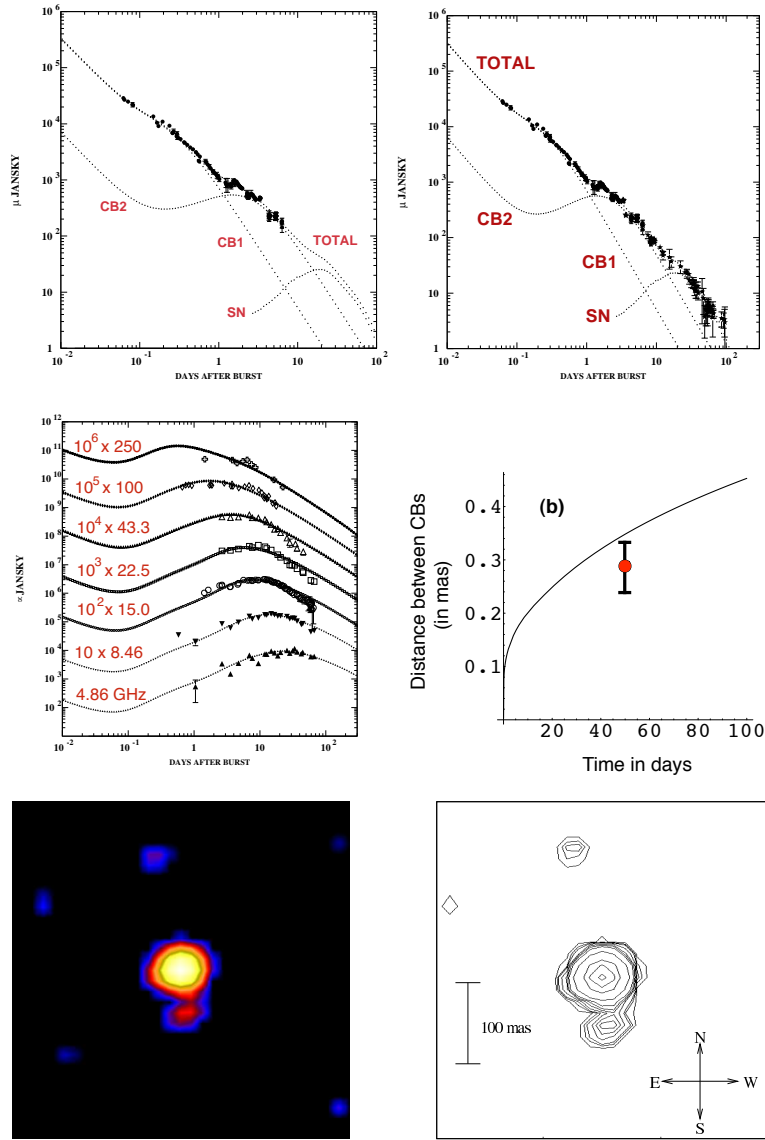


Figure 6: Left to right and top to bottom. a) and b) The R-band AG of GRB 030329. A micro-Jansky is  $10^{-29}$  erg cm $^{-2}$  s $^{-1}$ . a) Six days of data are used to predict the next  $\sim 100$  days, and the SN contribution. b) The SN is seen. c) The radio afterglows of GRB 030329. d) The predicted and observed inter-CB *superluminal* angle in this GRB. (e,f): SN1987A and its two ‘mystery spot’ CBs<sup>12</sup>). The motion of the Northern one was superluminal.



250 keV, evolving later to  $T(t) \sim t^{-2}$ . A pulse's shape at fixed  $E$  is well fit by:

$$\left. \frac{dN}{dt} \right|_E \approx \Theta[t] e^{-[\Delta t(E)/t]^2} \left\{ 1 - e^{-[\Delta t(E)/t]^2} \right\}; \quad \frac{\Delta t(E_1)}{\Delta t(E_2)} \approx \left[ \frac{E_2}{E_1} \right]^{\frac{1}{2}}, \quad (4)$$

with  $\Delta t \sim \mathcal{O}(1\text{s})$  at  $E \sim E_p$ . Eq. (4) reflects an approximate spectro-temporal correlation whereby  $E dN/(dE dt) \approx F[E t^2]$ , which we call the  $E t^2$  'law'.

The values of  $E_p$ ; of the isotropic-equivalent energy and luminosity,  $E_\gamma^{\text{iso}}$  and  $L_p^{\text{iso}}$ ; of a pulse's rise-time  $t_{\text{rise}}$ ; or of its 'lag-time'  $t_{\text{lag}}$  (a measure of how a pulse peaks at a later time in a lower energy interval) vary from GRB to GRB over orders of magnitude. But they are strongly correlated, as shown in Figs. (7a-d). It is patently obvious that such an organized set of results is carrying a strong and simple message, which we shall decipher.

X-ray flashes (XRFs) are lower-energy kinsfolk of GRBs. They are defined by having  $E_p < 50$  keV. Their pulses are wider than the ones of GRBs and their overlap is more pronounced, since the total durations of (multi-pulse) XRFs and GRBs are not significantly different. In fig. 7e I show the time at which the single pulse of XRF 060218 peaked (measured from the start of the count-rate rise) as measured in different energy intervals. This is an impressive validation of the  $E t^2$  law (the red line), also screaming for a simple explanation.

Analytical expressions summarizing the behaviour of GRB and XRF afterglows in time (from seconds to months) and frequency (from radio to X-rays) do exist (DDD02/03), but they are somewhat more complex than Eqs. (3,4). The typical AG behaviour is shown in fig. 7f, as a function of frequency, at 1, 10... 300 days after burst (the value of  $p$  is  $\sim 2.2 \pm 0.2$ ). This simple figure reflects a rich behaviour in time and frequency. 'Chromatic bends' (called 'breaks' in the literature) are an example. At a fixed time, the spectra steepen from  $\sim \nu^{-0.5}$  to  $\sim \nu^{-1.1}$  at the dots in the figure. Around a given frequency, such as the optical one marked by a dotted line, the optical spectrum makes this same transition as a function of time (at  $t \sim 3\text{d}$ , for the parameters of this example), while the spectral shape at X-ray frequencies stays put.

### 3.1 The Swift era

Physicists, unlike ordinary year-counting mortals, live in 'eras'. Many are waiting for the LHC era or the Plank era, GRB astronomers are in their 'Swift era'. Various satellites are currently contributing to a wealth of new data on GRBs and XRFs. Swift is one of them. Within 15 seconds after detection, its 15-150 keV Burst Alert Telescope sends to ground a 1 to 4 arcmin position estimate, for use by robotic optical ground telescopes. In 20 to 75 s, Swift slews to bring the burst location into the field of view of its 0.3-10 keV X-ray Telescope and its 170-650 nm UV/Optical Telescope. With nominal celerity, Swift has filled a gap in GRB data: the very 'prompt' X-ray and optical radiations.

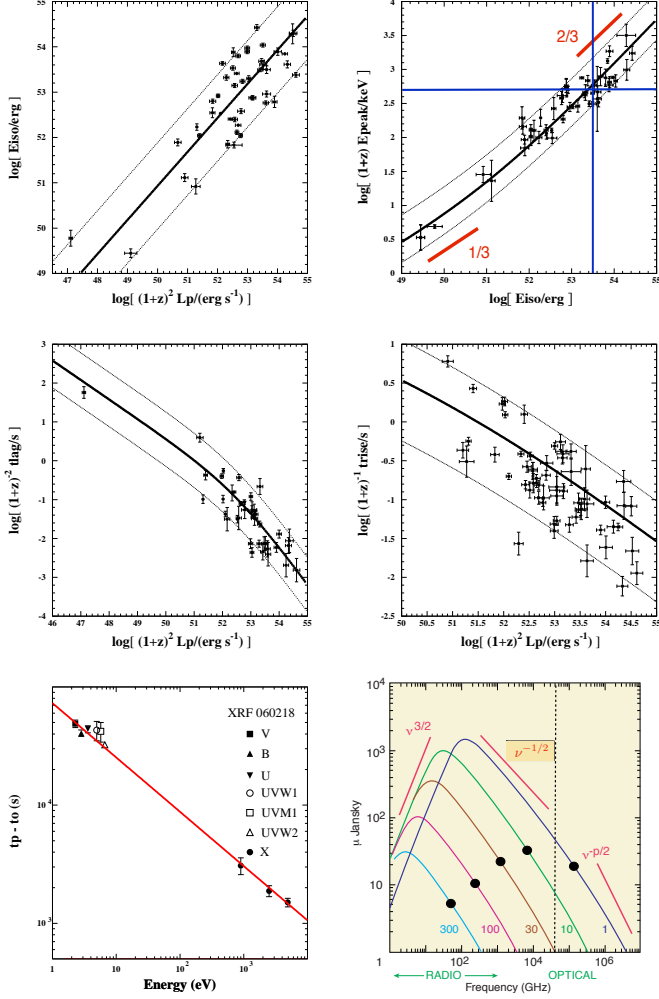


Figure 7: Left to right and top to bottom: a) The  $[E_{\gamma}^{\text{iso}}, L_p^{\text{iso}}]$  correlation. b) The  $[E_p, E_{\gamma}^{\text{iso}}]$  correlation. The limiting slopes are in red, the central predictions in blue. c) The  $[t_{\text{lag}}, L_p^{\text{iso}}]$  correlation. d) The  $[t_{\text{min}}^{\text{rise}}, L_p^{\text{iso}}]$  correlation. The data are for Swift-era GRBs of known  $z$ . e) The peak times of the one-pulse X-ray flash XRF 060218 at different energy intervals. f) A typical AG spectrum at different number of days after the burst (1, 10, ... 300). In the figure  $p/2 \sim 1.1$ .

Swift has established a *canonical behaviour* of the X-ray and optical AGs of a large fraction of GRBs. The X-ray fluence decreases very fast from a ‘prompt’ maximum. It subsequently turns into a ‘plateau’. After a time of  $\mathcal{O}(1d)$ , the fluence bends (has a ‘break’, in the usual parlance) and steepens to a power-decline. In fig. 8a, this is shown for a Swift GRB. This bend is achromatic: the UV and optical light curves vary in proportion to it. Although all this is considered a surprise, it is not. In fig. 8b I show a pre-Swift AG and its interpretation in two models. In fig. 8c one can see that the bend of this GRB was achromatic. Even the good old GRB 980425, the first to be clearly associated with a SN, sketched a canonical X-ray light curve, see fig. 8d.

The  $\gamma$  rays of a GRB occur in a series of *pulses*, 1 and 2 in the examples of fig. 5. Swift has clearly established that somewhat wider X-ray *flares* coincide with the  $\gamma$  pulses, having, within errors, the same start-up time. On occasion, even wider optical *humps* are seen, as in fig. 9a. The X-ray counterpart of the second hump in this figure is clearly seen in fig. 9b. In an XRF the X-ray flares can be very wide, as in the one-flare example of fig. 10a. In such a case, the accompanying optical ‘humps’ peak very late, at  $t = \mathcal{O}(1d)$ , as in fig. 10b. All these interconnected  $\gamma$ -pulses, X-ray flares and optical humps are described by Eqs. (3,4). They are obviously manifestations of a common underlying phenomenon, which we shall dig out. Finally, Swift has discovered that not all X-ray light curves are smooth after the onset of their fast decay, as the one in fig. 10a is. Well after  $\gamma$  pulses are no longer seen, relatively weak X-ray flares may still be observable, as is the case in figs. 9c,10d.

#### 4 Breath-taking entities: the astrophysical jets of cannonballs

A look at the web –or at the sky, if you have the means– results in the realization that jets are emitted by many astrophysical systems. One impressive case is the quasar Pictor A, shown in figs. (11a,b). *Somehow*, its active galactic nucleus is discontinuously spitting *something that does not appear to expand sideways before it stops and blows up*, having by then travelled almost  $10^6$  light years. Many such systems have been observed. They are very relativistic: the Lorentz factors (LFs)  $\gamma \equiv E/(mc^2)$  of their ejecta are typically of  $\mathcal{O}(10)$ . The mechanism responsible for these mighty ejections —suspected to be due to episodes of violent accretion into a very massive black hole— is not understood.

In our galaxy there are ‘micro-quasars’, whose central black hole’s mass is a few  $M_\odot$ . The best studied is GRS 1915+105. In a non-periodic manner, about once a month, this object emits two oppositely directed *cannonballs*, travelling at  $v \sim 0.92 c$ . When this happens, the continuous X-ray emissions —attributed to an unstable accretion disk— temporarily decrease. Another example is the  $\mu$ -quasar XTE J1550-564, shown in fig. 11c. The process reminds one of the blobs thrown up as the water closes into the ‘hole’ made by a stone dropped onto

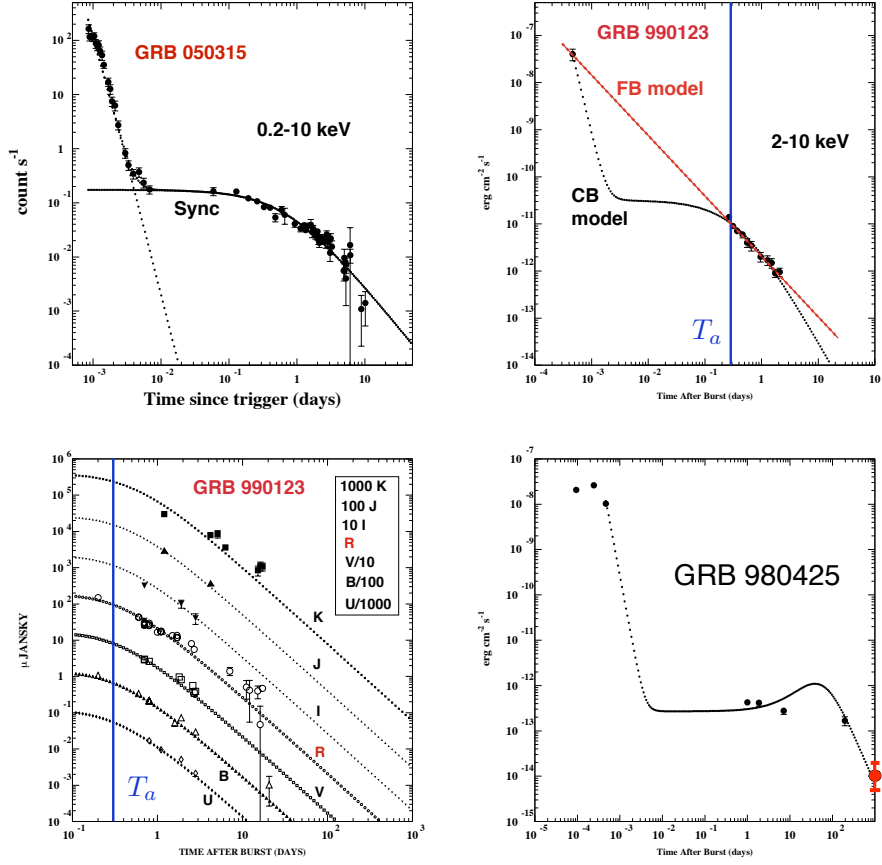


Figure 8: Right to left and top to bottom. a) The canonical 0.2-10 keV X-ray light curve of GRB 050315, fit to the CB model. b) Pre-SWIFT predictions for the 2-10 keV X-ray AG in the CB (DDD02) and fireball <sup>13)</sup> models, compared to data for GRB 990123. c) Broad band optical data on GRB 990123, fit in the CB model (DDD03). The ‘bend’ in (b) and (c) is due to the CBs’ deceleration, and is achromatic. d) The X-ray light curve of GRB 980425 showing a very pronounced ‘canonical’ behaviour and what we called (DDD02) a long ‘plateau’. The last (red) point postdates the original figure.

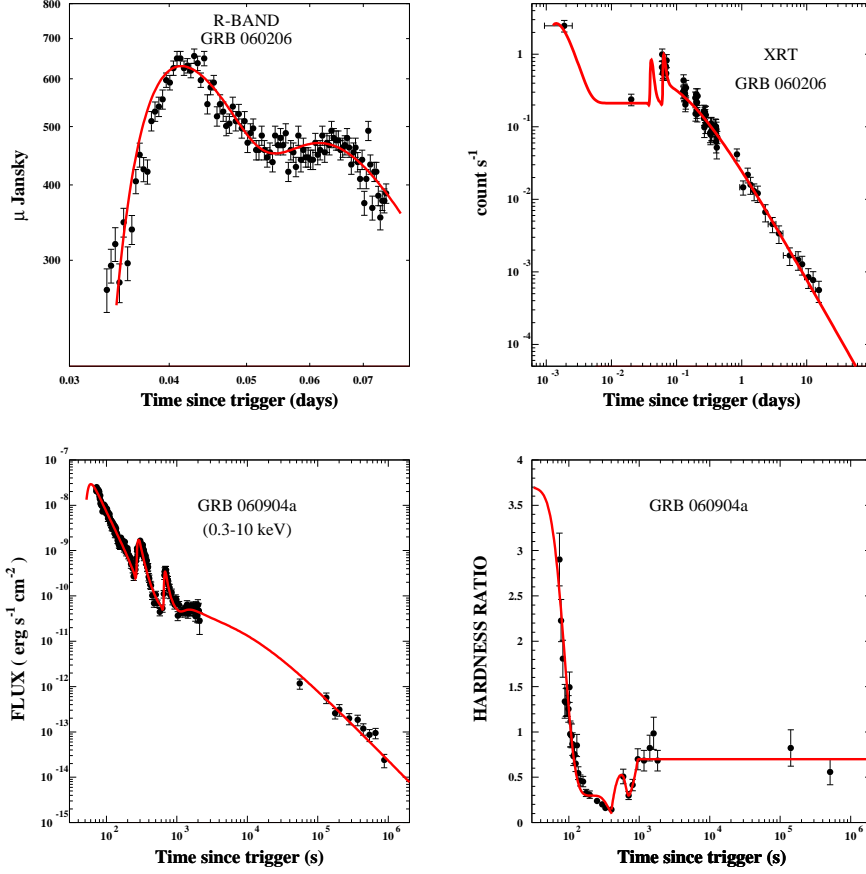


Figure 9: Left to right and top to bottom: a) Early R-band light curves of GRB 060206. b) Its X-ray light curve. c) The X-ray light curve of GRB 060904a with its late flares: the progressively dying pangs of its accreting engine. d) The hardness ratio of GRB 060904a traces the ‘prompt’ ICS pulses of its light curve, settling to a constant as SR becomes dominant in the ‘afterglow’. The above understanding of all these data is specific to the CB model.

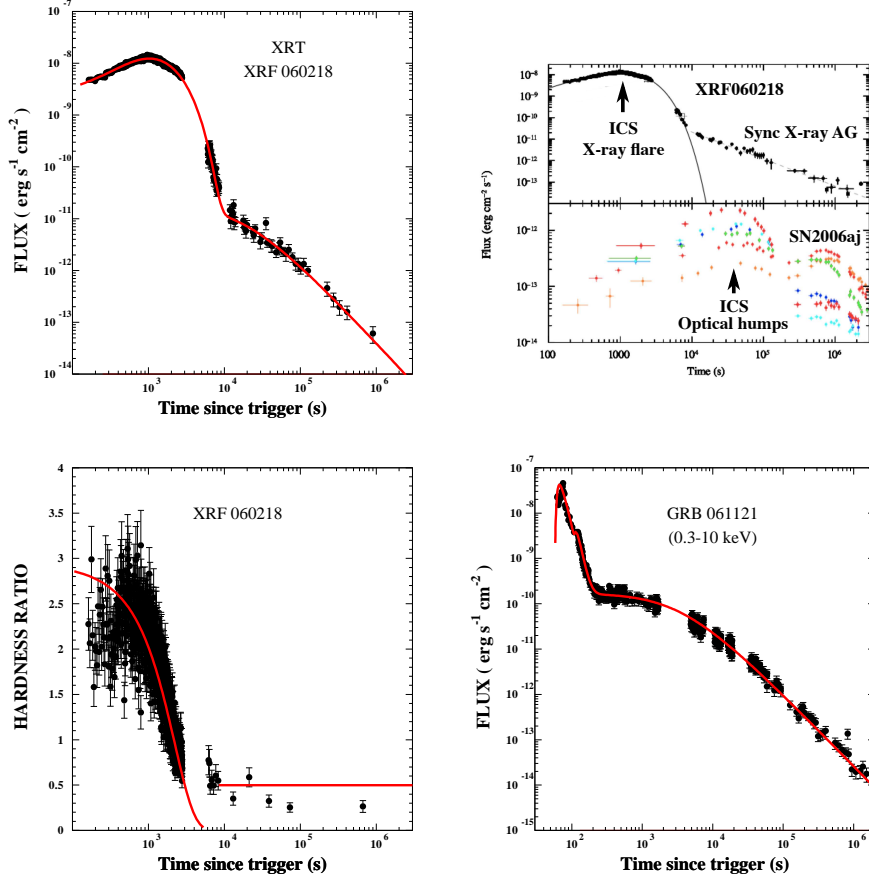


Figure 10: Left to right and top to bottom: a) The X-ray light curve of XRF 060218. b) Data on XRF 060218/SN2006aj. Upper part: the 0.3-10 keV SWIFT-XRT light curve, with fits by Campana et al. <sup>14)</sup>. Lower part: UVO light curves. In our model, the X-ray flare and optical humps are made by ICS by a single CB. c) The hardness ratio of XRF 060218. d) The extensive X-ray light curve of GRB 061121. The lines in (a,c,d) are CB-model fits.

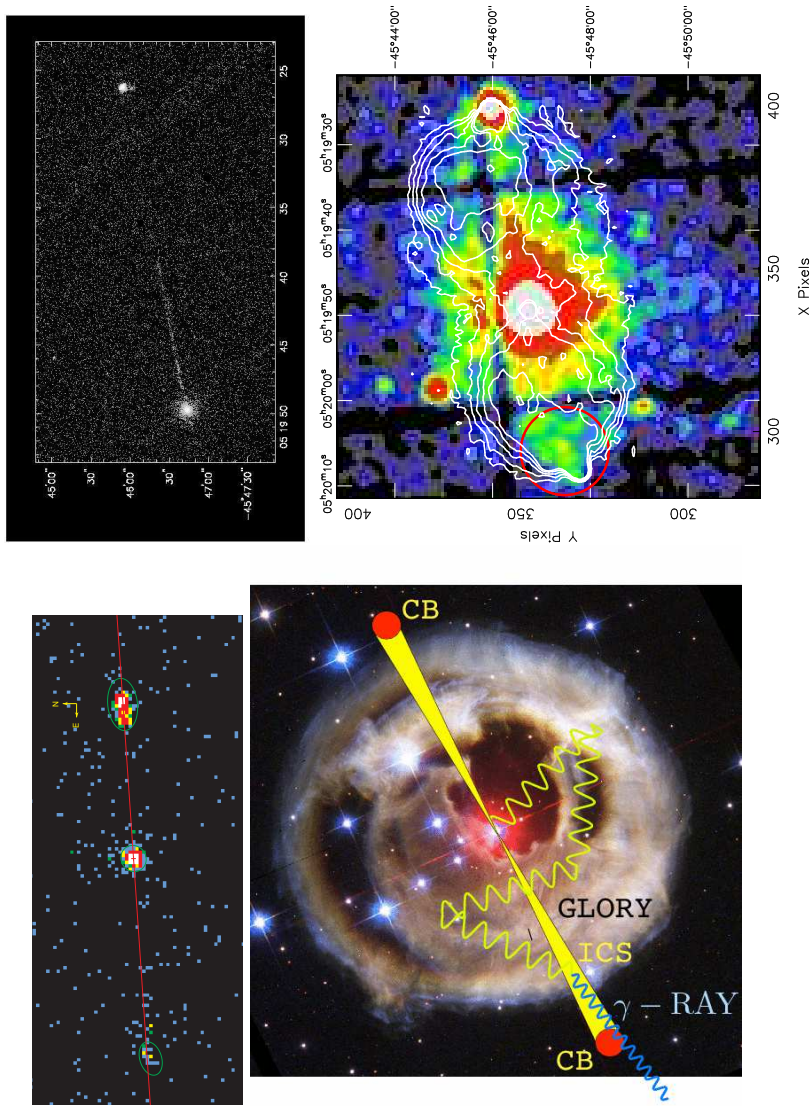


Figure 11: Left to right and top to bottom. a) and b) X-ray images of Pictor A. b) Image centred at the leftmost spot in (a) and superimposed on VLA radio contours. c) Two relativistic CBs emitted in opposite directions by the microquasar XTE J1550-564, seen in X-rays. d) HST picture from 28 October 2002 of the *glory*, or light echo, of a pre-supernova outburst of the red supergiant V838 Monocerotis, doctored with some CB-model art-work.

its surface, but it is not understood; for quasars and  $\mu$ -quasars, the ‘cannon’s’ relativistic, general-relativistic, catastrophic, magneto-hydro-dynamic details remain to be filled in! Atomic lines of many elements have been seen in the CBs of  $\mu$ -quasar SS 433. Thus, at least in this case, the ejecta are made of ordinary matter, and not of a fancier substance, such as  $e^+e^-$  pairs.

## 5 The Cannonball Model: summary

The ‘cannon’ of the CB model is analogous to the ones of quasars and microquasars. In an *ordinary core-collapse* SN event, due to the parent star’s rotation, an accretion disk is produced around the newly-born compact object, either by stellar material originally close to the surface of the imploding core, or by more distant stellar matter falling back after the shock’s passage<sup>15, 16)</sup>. A CB made of *ordinary-matter plasma* is emitted, as in microquasars, when part of the accretion disk falls abruptly onto the compact object. *Long-duration* GRBs and *non-solar* CRs are produced by these jetted CBs. To agree with observations, CBs must be launched with LFs,  $\gamma_0 \sim 10^3$ , and baryon numbers  $N_B = \mathcal{O}(10^{50})$ , corresponding to  $\sim 1/2$  of the mass of Mercury, a miserable  $\sim 10^{-7}$ th of a solar mass. Two jets, each with  $n_{CB} = \langle n_{CB} \rangle \sim 5$  CBs, carry

$$E_{\text{jets}} = 2 n_{CB} \gamma_0 N_B m_p c^2 \sim 1.5 \times 10^{51} \text{ erg}, \quad (5)$$

comparable to the energy of the SN’s non-relativistic shell, that is  $\mathcal{O}(1\%)$  of the explosion’s energy,  $\sim 98\%$  of which is carried away by thermal neutrinos.

We have seen that long GRBs are indeed made by SNe, as advocated in the CB model well before the pair GRB030329/SN2003dh convinced the majority. But do SNe emit cannonballs? Until 2003<sup>17)</sup>, there was only one case with data good enough to tell: SN1987A, the core-collapse SN in the LMC, whose neutrino emission was seen. Speckle interferometry data taken 30 and 38 days after the explosion<sup>12)</sup> did show two back-to-back relativistic CBs, see fig. 6e,f. The approaching one was *superluminal*: seemingly moving at  $v > c$ .

A summary of the CB model is given in Fig. 12. The ‘*inverse*’ *Compton scattering* (ICS) of light by electrons within a CB produces a forward beam of higher-energy photons: a pulse of a GRB or an XRF. The target light is in a temporary reservoir: the *glory*, illuminated by the early SN light and illustrated by analogy in fig. 11d. A second mechanism, *synchrotron radiation* (SR), takes over later and generally dominates the AG. The  $\gamma$  rays ionize the ISM on the CB’s path. The CBs collide with the ISM electrons and nuclei, boosting them to cosmic ray status. The ISM penetrating a CB’s plasma creates turbulent magnetic fields within it. The ISM electrons moving in this field emit the mentioned SR. This paradigm accounts for all properties of GRBs and CRs.

The observed properties of a CB’s radiation depend crucially on the angle



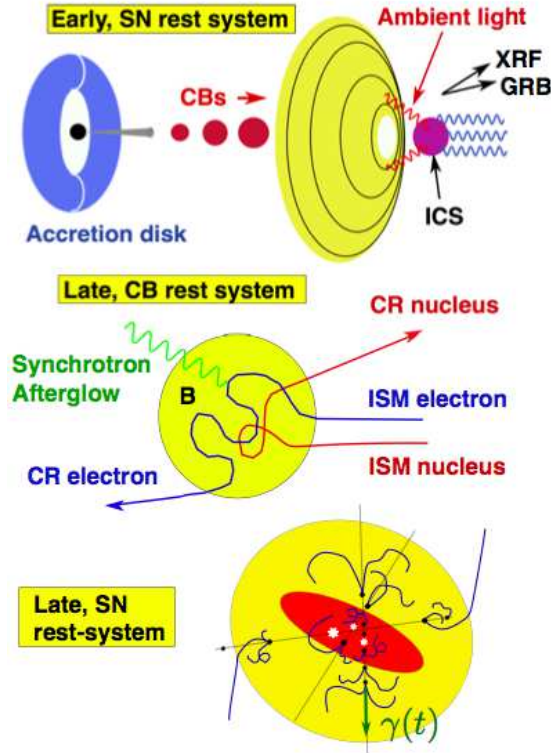


Figure 12: The CB model of GRBs, XRFs and CRs. A core-collapse SN results in a (black) compact object, a fast-rotating torus of non-ejected material and a (yellow) shell of non-relativistic ejecta. Matter (not shown) episodically accreting into the central object produces two narrowly collimated beams of CBs; some of the ‘Northern’ CBs are depicted. As the CBs move through the *glory* of non-radial light surrounding the star, they forward Compton up-scatter its photons to GRB or XRF energies, depending on how close the line of sight is to the CBs’ direction. Each CB produces a GRB ‘pulse’. Later, a CB gathers and scatters ISM particles, which are isotropized by its inner magnetic field. In the SN rest system the particles are boosted by the CB’s motion: they have become CRs. The synchrotron radiation of the gathered electrons is the late AG of the GRB or XRF. As the CBs’ collisions with the ISM slow them down, the CBs generate CRs all along their trajectories, in the galaxy and its halo. CRs are also forward-produced, diffusing thereafter in the local magnetic fields.

$\theta$  of its motion relative to the line of sight to the observer, via the Doppler factor

$$\delta = 1/[\gamma(1 - \beta \cos \theta)] \approx 2\gamma/(1 + \theta^2\gamma^2) \quad (6)$$

by which a photon's energy is boosted from the CB's rest system to that of a (cosmologically nearby) observer. For an isotropic emission in the CB's system, the observed photon number, energy flux and luminosity are  $\propto \delta, \delta^3, \delta^4$ , respectively, just as in a  $\nu$  beam from  $\pi$  decay. That makes GRBs observable only extremely close to one of their bipolar CB axes,  $\theta = \mathcal{O}(1/\gamma) \sim 1$  mrad [typically  $\gamma(t=0) = \gamma_0 \sim \delta_0 \sim 10^3$ ; and AGs are observed till  $\gamma(t) \sim \gamma_0/2$ ].

The relation between CB travel-time in the host galaxy,  $dt_* = dx/(\beta c)$ , and observer's time,  $t$ , is  $dt_*/dt = \gamma\delta/(1+z)$ . Stop in awe at this gigantic factor: a CB whose AG is observed for 1 day may have travelled for  $\mathcal{O}(10^6)$  light days, what a fast-motion video! A CB with  $\theta = 1/\gamma = 10^{-3}$  moves in the sky at an apparent transverse velocity of  $2000c$ , yet another large Doppler aberration.

## 6 GRB afterglows in the CB model

Historically, two GRB phases were distinguished: a prompt one, and the *afterglow*. Swift data have filled the gap, there is no longer a very clear distinction. Nor is there a profound difference between the CB-model's radiation mechanisms, since synchrotron radiation is but Compton scattering on virtual photons and, in a universe whose age is finite, all observed photons were virtual.

In the understanding of GRBs in the CB model, SR-dominated AGs came first. The CB-model AG analysis is strictly a 'model': it contains many simplifications. But the comparison with data determines the distributions of the relevant parameters. Given these, the predictions for CRs and for the ICS-dominated phase of GRBs (such as all properties of the  $\gamma$ -ray pulses) involve only independent observations, basic physics and no 'modeling'. For the reader who might want to move to the more decisive sections, I anticipate the contents of this one. The distribution of  $\gamma_0$  and  $\gamma_0 \delta_0$  values of pre-Swift GRBs are shown in fig. 13a,b. The radius of a CB evolves as in fig. 13d. A CB does not expand inertially; for most of its trajectory it has a slowly changing radius, as a common *cannonball* does. The baryon number of observed CBs is of  $\mathcal{O}(10^{50})$ .

To determine the fate of a CB, we make the following assumptions. CBs initially expand at  $\beta_s c = \mathcal{O}(c/\sqrt{3})$ , the relativistic speed of sound, swiftly becoming spherical in their rest system and losing memory of their initial size. For the CB's baryon number returned by the analysis, this means that CBs become 'collisionless' fast: their nuclei and electrons do not often collide with the ISM ones they encounter. Hadron and Thompson cross sections being similar, CBs also become transparent, except to long radio waves, losing their radiation pressure. In agreement with first-principle calculations of the relativistic merger of two plasmas<sup>18)</sup>, a chaotic magnetic field is generated within a CB

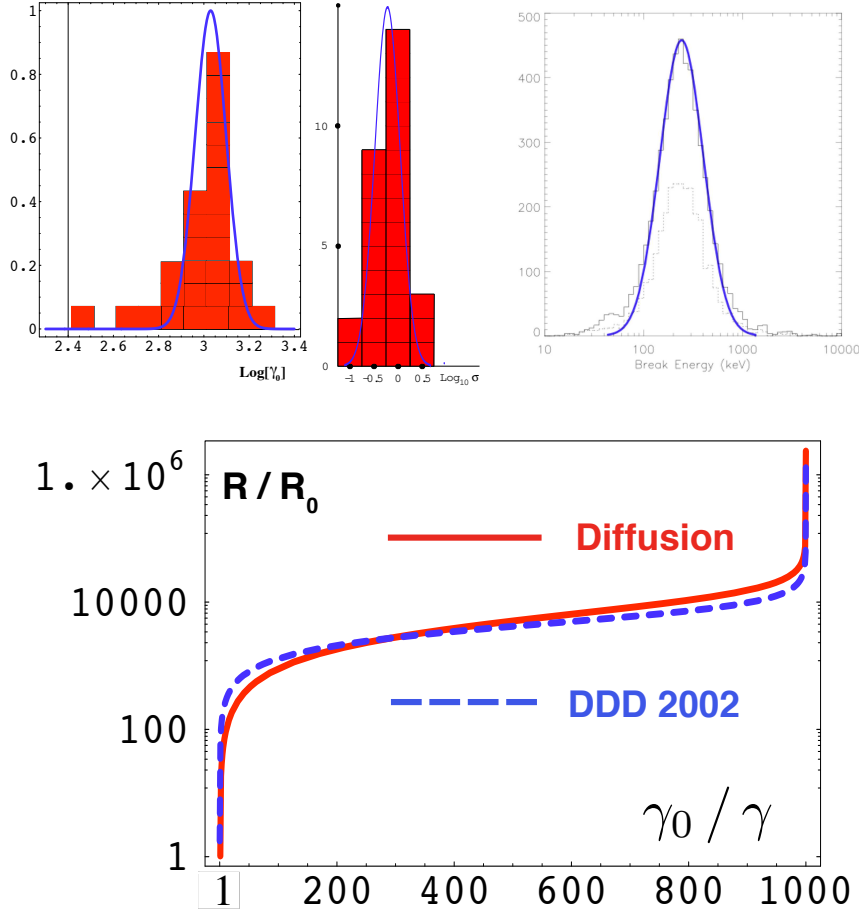


Figure 13: Right to left, top to bottom. a) The distribution of  $\text{Log}_{10}(\gamma)$  for a score of pre-Swift GRBs of known  $z$ . b) The distribution of  $\sigma \equiv \text{Log}_{10}(\gamma\delta/10^6)$  for the same GRBs, also extracted from the analysis of their AGs. c) The distribution of peak or ‘break’ energies in the spectrum of many pre-Swift GRBs. The line is the CB-model prediction, based on Eq. (12) and the observed  $\sigma$  distribution. d) The behaviour of  $R(\gamma/\gamma_0)$  in two extremes (diffusive or instantaneous) for the way the intercepted ISM ions reexit a CB. The coasting behaviour at  $R \sim R_c$  and final blow-up at  $\gamma \rightarrow 1$  are of the form  $R \approx R_c (\gamma_0/\beta\gamma)^{2/3}$ .

by the ISM particles it sweeps in. In accordance with observations of similar plasmas (such as the ISM itself and the CRs it contains) the CB's magnetic field is in energy equipartition with the impinging ISM, resulting in:

$$B_{\text{CB}}(\gamma) = 3 \text{ G } (\gamma/10^3) [n/(10^{-2} \text{ cm}^{-3})]^{1/2}, \quad (7)$$

where  $n$  is the ISM baryonic number density, normalized to a typical value in the 'superbubbles' in which most SNe and GRBs are born.

In a CB's rest system the motion of its constituents is an inertial memory of the initial radial expansion, whose kinetic energy is larger than the one of the CB's magnetic field. An ISM proton entering a CB will meander in its magnetic field and be isotropically reemitted (in the CB's rest system). The rate of radial momentum loss per unit surface is a surface pressure countering the expansion. We assume that the dominant effect of this pressure is to counteract the expansion. We use Newton's law to compute the ensuing radial deceleration and the CB's radius  $R(\gamma)$ . The results are shown in fig. 13d. A CB initially expands quasi-inertially. It subsequently settles into a slowly evolving radius till it blows up as its motion becomes non-relativistic (DD06), obeying:

$$R(\gamma) \approx R_c (\gamma_0/\beta\gamma)^{2/3}, \text{ with } R_c = \mathcal{O}(10^{14} \text{ cm}), \text{ for typical parameters.} \quad (8)$$

This is a complex problem, and ours is a big simplification, once assessed by a cunning referee as "almost baron Munchhausen". Yet, the result describes the surprising 'jet self-focusing' observed, e.g., in Pictor A, see fig. 11a.

The collisions with the ISM continuously decelerate a CB. For a given  $R(t)$  and ISM baryon number per unit volume  $n$ , energy-momentum conservation dictates the explicit form of the CB's diminishing Lorentz factor  $\gamma(t)$ . Typically  $\gamma(t)$  is roughly constant for a day or so of observer's time, steepening to  $\propto t^{-1/4}$  thereafter. During the short  $\gamma$ -ray emission time,  $\gamma(t) \approx \gamma_0$ .

We assume that practically all of the energy of the ISM electrons (of number density  $n_e \simeq n$ ) entering a CB is reemitted fast in the form of SR, so that the corresponding observed frequency-integrated AG power per unit area is  $dF/(dt d\Omega) = \pi R^2 n_e m_e c^3 \gamma^2 \delta^4 / (4\pi D_L^2)$ , with  $D_L$  the luminosity distance. The CB deceleration law, dictated by energy-momentum conservation, is equally simple:  $M_0 \gamma_0 d\gamma = -\pi R^2 n m_p \gamma^3 dx$ , for an H-dominated ISM and in the extreme in which the re-emission time of protons is long on the scale of the CB's deceleration time. For constant  $n$ , the distance travelled by a CB is:

$$x(\gamma) \approx L \left[ (\gamma_0/\gamma)^{2/3} - 1 \right], \quad L = 3 N_B / (2\pi R_c^2 n \gamma_0^3) = 180 \text{ pc}, \quad (9)$$

where the number is for  $N_B = 10^{50}$ ,  $n = 10^{-2} \text{ cm}^{-3}$ ,  $R_c = 10^{14} \text{ cm}$ ,  $\gamma_0 = 10^3$ . Given all this, it appears easy to extract from an AG's normalization and shape the values of  $\theta$ ,  $\gamma_0$  and  $N_B$ , if one trusts the estimate of  $R(\gamma)$  and uses a typical  $n$ . Limited observational information makes life a bit harder.

The spectrum of fig. 7f is actually the one predicted by the CB model, illustrated for a typical choice of parameters. The chromatic ‘bends’ shown as dots in this figure, for instance, are ‘injection bends’: the typical SR energy, in the CB’s magnetic field, of the electrons entering it, at time  $t$ , with a (relative) LF  $\gamma = \gamma(t)$ . The small portion of the spectrum above the bend is emitted by a tiny fraction of electrons ‘Fermi-accelerated’ in the CB’s turbulent magnetic fields to a pre-synchrotron-cooling spectrum  $E_e^{-p}$ , with  $p \sim 2.2$ . The prediction fits with no exception the AGs of the first score of well measured GRBs (DDD02/03) of known  $z$ . But only on rare occasions can one clearly see in an AG the contributions of the various CBs seen in the  $\gamma$ -ray count rate (a counterexample is the GRB of figs. 5b, 6a,b). Thus, generally, the parameters extracted from AG fits refer to a dominant CB or to an average over CBs.

After an observer’s day or so, the optical and X-ray AG are typically SR-dominated, are above the injection bend, and are of the approximate form:

$$F_\nu \propto n_{\text{CB}} n^{1.05} R_c^2 \gamma^{2.3} \delta^{4.1} \nu^{-1.1}, \quad (10)$$

where the unwritten proportionality factors, such as  $D_L^{-2}$ , are known. From a fit to the shape of  $F_\nu(t)$  one obtains  $\theta\gamma_0$  and the combination  $L$  of Eq. (9). At late times  $F_\nu \propto \gamma(t)^{6.4} \propto \gamma_0^{6.4}$  with a coefficient determined by the other fit parameters. The value of  $\gamma_0$  is extracted from the 6.4 root of the inverse of Eq. (10), so that, for a result within a factor of 2, one can tolerate large errors in the chosen  $n$  or in the estimate of  $R_c^2$ . Trusting these, one can extract  $N_b$  from  $L$ , perhaps with an uncertainty of one order of magnitude<sup>1</sup>. Eq. (10) has been used to fit, after the early fast fall-off, the X-ray and optical data of figs. 8,9,10. The required form of  $\gamma(t)$  is Eq. (8), supplemented by the relation between CB’s mileage and observer’s time, see the end of Sec. 5.

## 7 A GRB’s $\gamma$ rays in the CB model (DD06)

A pulse of a GRB is made by a CB crossing the parent star’s *glory*. The glory is a reservoir of non-radially directed light, fed by the parent star’s luminosity, as in the artist’s view of fig. 11d. For the best studied GRB-associated SN, 1998bw, and for  $\mathcal{O}(1d)$  after the explosion, the luminosity was  $L_{\text{SN}} \sim 5 \times 10^{52}$  erg/s, in photons of typical energy  $E_i \sim 1$  eV. We adopt these values as ‘priors’ (parameters to be used in calculations, but independent of the CB model). Massive stars destined to ‘go supernova’ eject solar-mass amounts of matter in successive explosions during their last few thousand pre-SN years. At the ‘close’ distances of  $\mathcal{O}(10^{16}$  cm) relevant here, these stellar coughs generate a thick layer of ‘wind-fed’ material with an approximate density profile  $\rho \propto r^{-2}$

---

<sup>1</sup>This is what we did in DDD02/03 but not quite what we wrote. I am indebted to J. Steinberger for noticing this error.

and normalization  $\rho r^2 \sim 10^{16} \text{ g cm}^{-1}$ , the last prior we need. The very early UV flash of the SN suffices to ionize the wind-fed matter. The Thompson cross section  $\sigma_T$  is such that this matter is semitransparent:  $\sigma_T \rho r^2 / m_p = 4 \times 10^{15}$  cm. This means that the number of times a SN photon reinteracts on its way out –becoming ‘non-radial’– is of  $\mathcal{O}(1)$ , and that the number density of such photons is  $n_\gamma(r) \sim L_{\text{SN}} / (4\pi r^2 c E_i)$ . From emission-time to the time it is still one  $\gamma$ -ray interaction length inside the ‘wind’, a CB has travelled for

$$t_{\text{tr}}^w = (0.3 \text{ s}) \frac{\rho r^2}{10^{16} \text{ g cm}^{-1}} \frac{1+z}{2} \frac{10^6}{\gamma_0 \delta_0} \quad (11)$$

of observer’s time. That is a typical  $\gamma$ -ray pulse rise-time in a GRB, and the reason why, closing the loop, distances of  $\mathcal{O}(10^{16} \text{ cm})$  were relevant.

In the collapse of a rotating star, material from ‘polar’ directions should fall more efficiently than from equatorial directions. The CBs would then be emitted into relatively empty space. We assume that the wind-material is also under-dense in the polar directions. This is not the case for the glory’s photons, which have been scattered by the wind’s matter, and partially isotropised. During the production of  $\gamma$ -rays by ICS,  $\gamma \simeq \gamma_0$ .

Consider an electron, comoving with a CB at  $\gamma = \gamma_0$ , and a photon of energy  $E_i$  moving at an angle  $\theta_i$  relative to  $\vec{r}$ . They Compton-scatter. The outgoing photon is viewed at an angle  $\theta$ . Its energy is totally determined:

$$E_p = \frac{\gamma \delta}{1+z} (1 + \cos \theta_i) E_i = (250 \text{ keV}) \sigma \frac{1 + \cos \theta_i}{1/2} \frac{E_i}{1 \text{ eV}}, \quad \sigma \equiv \frac{\gamma \delta}{10^6} \frac{2}{1+z}, \quad (12)$$

where I set  $\beta \approx 1$  and, for a *semi* transparent wind,  $\langle \cos \theta_i \rangle \sim -1/2$ . For pre-Swift GRBs  $\langle z \rangle \approx 1$  and, for the typical  $\gamma$  and  $\delta$ ,  $E = 250 \text{ keV}$ , the average peak or ‘break’ energy in Eq. (3). From the fits to the AGs of the subset of known  $z$ , we could determine the distribution of  $\sigma$  values, see fig. 13b. Its fitted result is used in Eq. (12) to predict the overall  $E_p$  distribution, see fig. 13c.

The rest of the properties of a GRB’s pulse can be derived on similarly trivial grounds and with hardly more toil. During the GRB phase a CB is still expanding inertially at a speed  $\beta_s c$ . It becomes transparent when its radius is  $R_{\text{tr}} \sim [3 \sigma_T N_B / (4\pi)]^{1/2}$ , at an observer’s time very close to that of Eq. (11), for typical parameters. One can simply count the number of ICS interactions of a CB’s electrons with the glory, multiply by their energy, Eq. (12), and figure out the isotropic-equivalent energy deduced by an observer at an angle  $\theta$ :

$$E_\gamma^{\text{iso}} \simeq \frac{\delta^3 L_{\text{SN}} N_{\text{CB}} \beta_s}{6 c} \sqrt{\frac{\sigma_T N_B}{4 \pi}} \sim 3.2 \times 10^{53} \text{ erg}, \quad (13)$$

where the number is for our typical parameters, and agrees with observation.

### 7.1 Is it Inverse Compton Scattering ...

The  $\gamma$  and  $\delta$  dependance in Eqs. (12,13) is purely ‘kinematical’, but specific to ICS: it would be different for self-Compton or synchrotron radiation. To verify that the  $\gamma$  rays of a GRB are made by ICS, as proposed <sup>19)</sup> by Shaviv and Dar, we may look at the correlations <sup>20, 21)</sup> between GRB observables.

In the CB model, the  $(\gamma, \delta, z)$  dependences of the peak isotropic luminosity of a GRB,  $L_p^{\text{iso}}$ ; its pulse rise-time,  $t_{\text{rise}}$ ; and the lag-time between the peaks of a pulse at different energies,  $t_{\text{lag}}$ ; are also simply derived <sup>21)</sup> to be:

$$(1+z)^2 L_p^{\text{iso}} \propto \delta^4, \quad t_{\text{rise}} \propto (1+z)/(\gamma\delta), \quad t_{\text{lag}} \propto (1+z)^2/(\delta^2\gamma^2). \quad (14)$$

I have not specified the numerical coefficients in Eqs. (14), which are explicit, as in Eqs. (12,13). Of all the parameters and priors in these expressions, the one explicitly varying by orders of magnitude by simply changing the observer’s angle is  $\delta(\gamma, \theta)$ , making it the prime putative cause of case-by-case variability. For such a cause, Eqs. (13) and the first of (14) imply that  $E_\gamma^{\text{iso}} \propto [(1+z)^2 L_p^{\text{iso}}]^{3/4}$ . This is tested in fig. 7a. A most celebrated correlation is the  $[E_p, E_\gamma^{\text{iso}}]$  one, see Fig. 7b. It evolves from  $E_p \propto [E_\gamma^{\text{iso}}]^{1/3}$  for small  $E_p$ , to  $E_p \propto [E_\gamma^{\text{iso}}]^{2/3}$  for large  $E_p$ . This is because the angle subtended by a moving CB from its place of origin is  $\beta_s/\gamma$ , comparable to the beaming aperture,  $1/\gamma$ , of the radiation from a point on its surface. Integration over this surface implies that, for  $\theta \ll 1/\gamma$ ,  $\delta \propto \gamma$ , while in the opposite case  $\delta$  varies independently. The straight lines in fig. 7b are the central expectations of Eqs. (12,13), the data are fit to the predicted evolving power law. The predicted  $[t_{\text{lag}}, L_p^{\text{iso}}]$  and  $[t_{\text{rise}}, L_p^{\text{iso}}]$  correlations are tested in figs. 7c,d. The seal of authenticity of inverse Compton scattering —by a quasi-point-like electron beam— is unmistakable in all of this, QED.

### 7.2 ... on a Glory’s light ?

The ‘target’ photons subject to ICS by the CB’s electrons have very specific properties. Their number-density,  $n_\gamma(r) \propto L_{\text{SN}}/r^2$ , translates into the  $\sim t^{-2}$  late-time dependence of the number of photons in a pulse since, once a CB is transparent to radiation, ICS by its electrons simply ‘reads’ the target-photon distribution. As a CB exits the wind-fed domain, the photons it scatters are becoming more radial, so that  $1 + \cos\theta_i \rightarrow r^{-2} \propto t^{-2}$  in Eq. (12). For a semi-transparent wind material, which we have studied in analytical approximations and via Montecarlo, this asymptotic behaviour is reached fast and is approximately correct at all  $t$ . This means that the energies of the scattered photons evolve with observer’s time as  $t^{-2}$ : the ‘ $E t^2$  law’ of Eq. (4) and fig. 7e.

### 7.3 The pulse shape and the spectrum

The spectrum of a GRB, Eq. (3), and the time-dependence of its pulses, Eq. (4), describe the data well, and are actually analytical approximations to the results of ICS of an average CB on a typical glory. The spectrum of a semitransparent glory has a ‘thermal bremsstrahlung’ shape,  $dn_\gamma/dE_i \propto (T_i/E_i)^\alpha \text{Exp}[-E_i/T_i]$ , with  $\alpha \sim 1$  and  $T_i \sim 1$  eV. The first term in Eq. (3) is this same spectrum, boosted by ICS as in Eq. (12), by electrons comoving with the CB,  $E_e = \gamma m_e c^2$ . The second term is due to ICS by ‘knock-on’ electrons (generated while the CB is not yet collisionless) and electrons ‘Fermi-accelerated’ by the CB’s turbulent magnetic fields. They both have a spectrum  $dn_e/dE_e \propto E_e^{-\beta}$ , with  $\beta \sim 2$  to 2.2. They are a small fraction of the CB’s electrons, reflected in the parameter  $b$ , which we cannot predict. The temporal shape of a pulse has an exponential rise due to the CB and the windy material becoming transparent at a time  $\sim t_{\text{tr}}^w$ , see Eq. (11), the width of pulse (in  $\gamma$  rays) is a few  $t_{\text{tr}}^w$ , the subsequent decay is  $\propto t^{-2}$ . The time-energy correlations obey the ‘ $E t^2$  law’. All as observed.

### 7.4 Polarization

A tell-tale signature of ICS is the high degree of polarization. For a pointlike CB the prediction<sup>19)</sup> is  $\Pi \approx 2\theta^2 \gamma^2 / (1 + \theta^4 \gamma^4)$ , peaking at 100% at  $\theta = 1/\gamma$ , the most probable  $\theta$ , corresponding to  $90^\circ$  in the CB’s system. For an expanding CB,  $\Pi$  is a little smaller. For SR, which dominates the AGs at sufficiently late times, the expectation is  $\Pi \approx 0$ . The  $\gamma$ -ray polarization has been measured, with considerable toil, in 4 GRBs. It is always compatible, within very large errors, with 100%. The situation is unresolved<sup>22)</sup>. I shall not discuss it.

## 8 Detailed Swift light curves and hardness ratios

Swift has abundantly filled its goal to provide X-ray, UV and optical data starting briefly after the detection of a GRB: compare the Swift result of fig. 8a to the pre-Swift data in fig. 8b. In the CB-model description of the data in figs. 8,9,10, the abruptly falling signal is the tail of one or several  $\gamma$ -ray pulses or X-ray flares, produced by ICS and jointly described by Eqs. (3,4). The following ‘afterglow’, its less pronounced decay and subsequent achromatic ‘bend’ are due to the CBs’ synchrotron radiation, described by Eq. (10). Thanks to the quality of SWIFT data one can proceed to test these CB-model predictions in detail.

The two prompt optical ‘humps’ of GRB 060206 in fig. 9a are the ICS low-energy counterparts of its two late X-ray flares of fig. 9b, simultaneously fit by Eqs. (3,4). Swift provides a rough measure of a GRB’s spectrum: the *hardness ratio* of count rates in the [1.5-10] keV and [0.3-1.5] keV intervals. Given the case-by-case parameters of a CB-model fit to the [0.3-10] keV light



curve, one can estimate the corresponding hardness ratio <sup>23)</sup>. This is done in figs. 9c,d and 10a,c for GRB 060904 and XRF 060218, respectively. This last XFR is observed at a ‘large’ angle,  $\theta \sim 5$  mrad and a correspondingly small  $\delta_0$ , its single X-ray pulse is, in accordance with Eq. (11), relatively wide. The optical and UV counterparts of the X-ray pulse are clearly visible as the ‘humps’ in the optical data of fig. 10b. Given the ‘ $E t^2$ ’ law’ of Section 7.3, the pulse peak times at different frequencies are simply related:  $t_{\text{peak}} \propto E^{-1/2}$ . The prediction, an example of the ubiquitous  $1/r^2$  law of 3-D physics, is tested in fig. 7e. The peak fluxes at all frequencies are also related as dictated <sup>9)</sup> by Eq. (3). The adequacy of the CB model over many decades in flux and time is exemplified by the X-ray light curve of GRB 061121 in fig. 10d.

The predictions for the peak  $\gamma$ -ray energy of Eq. (12), its distribution as in fig. 13c, the GRB spectrum of Eq. (3), and the correlations of figs. 7a-d are clear proof that ICS is the prompt GRB mechanism. The test of the  $E t^2$  law in fig. 7e corroborates that the ‘target light’ becomes increasingly radially directed with distance: *Inverse Compton Scattering on a ‘glory’s light’ by the electrons in CBs is responsible for the  $\gamma$ -ray pulses of a GRB and their sister X-ray flares and optical humps.* The properties of the subsequent *synchrotron-dominated afterglows* are also in accordance with the CB model.

## 9 The GRB/SN association in the CB model

We have gathered very considerable evidence that the LFs and viewing angles of *observed* GRBs are  $\gamma_0 = \mathcal{O}(10^3)$  and  $\theta = \mathcal{O}(1)$  mrad. The fraction of GRBs beamed towards us is  $\sim \theta^2 = \mathcal{O}(10^{-6})$ . The number of such observed GRBs (with a hypothetical  $4\pi$  coverage) is a few a day. The same coverage would result in the observation of a few million core-collapse SN per day, in the visible Universe. These numbers are compatible with the extreme conclusion that *all* these SNe emit GRBs, but the estimates and errors are sufficient to accommodate a one order of magnitude smaller fraction, which would be compatible with most Type Ib/c emitting (long) GRBs.

## 10 Short Hard $\gamma$ -ray Bursts (SHBs)

SHBs share with (long) GRBs the properties not reflected in their name. A good fraction of SHBs have ‘canonical’ X-ray light curves. The origin of SHBs is not well established, in contrast to that of GRBs and XRFs. Clues to the origin and production mechanism of SHBs are provided by their similarity to long GRBs. The X-ray light curves of some well-sampled SHBs are ‘canonical’. The similarities suggest common mechanisms generating the GRB and SHB radiations. This is expected in the CB model, wherein both burst types are produced by highly relativistic, narrowly collimated, bipolar jets of CBs, ejected

in stellar processes<sup>19)</sup>. The mechanisms for their prompt and AG emissions (ICS and synchrotron) coincide with the ones of GRBs. The ‘engine’ is different; it is a core-collapse supernova for GRBs and XRFs, in SHBs it may be a merger (of two neutron stars or a neutron star and a black hole), the result of mass accretion episodes on compact objects in close binaries (e.g. microquasars), or phase transitions in increasingly compactified stars (neutron stars, hyper-stars or quark stars), induced by accretion, cooling, or angular-momentum loss.

In the CB model, the ‘master formulae’ describing prompt and afterglow emissions in long GRBs are directly applicable to SHBs, provided the parameters of the CBs, of the glory, and of the circumburst environment, are replaced by those adequate for SHBs. This results in a good description of the data<sup>24)</sup>.

## 11 Cosmic Rays in the CB model

In the CB model, CRs are as simple to understand as GRBs. If relativistic CBs are indeed ejected by a good fraction of core-collapse SNe, it is inevitable to ask what they do as they travel in the ISM. The answer is that they make CRs with the observed properties, simply by interacting with the constituents of the ISM, previously ionized by the  $\gamma$  rays of the accompanying GRB. Early in their voyage, CBs act as *Compton relativistic rackets*, in boosting a glory’s photon to  $\gamma$ -ray status. Analogously, all along their trajectories, CBs act as *Lorentz relativistic rackets*, in boosting an ISM nucleus or electron to CR status. Once again, the necessary input is two-fold. On the one hand, there are the properties of CBs: the average number of significant GRB pulses (or CBs) per jet (5), the  $\gamma_0$  distribution of fig. 13a, and the  $N_B \sim 10^{50}$  estimate. On the other hand, there are a few ‘priors’, items of information independent of the CR properties: the rate of core-collapse SNe, the relative abundances,  $n_A$  (of the elements of atomic number  $A$ ) in the ISM, and the properties of Galactic magnetic fields.

We shall see that the CB-model predictions for the normalization of CR spectra are correct to within a factor of  $\mathcal{O}(3)$ , while the ratios between elements are correct within errors. In figs. 1, 3 and 4a, the predictions have been made to adjust the data, not reflecting the common overall normalization uncertainty.

### 11.1 Relativistic rackets: The knees

Our simplest result concerns the ‘knees’ of the all-particle spectrum in fig. 1a and of the main individual elements in fig. 3. The essence of their understanding is kinematical and trivial. In an *elastic* interaction of a CB at rest with ISM electrons or ions of LF  $\gamma$ , the light recoiling particles (of mass  $m \approx A m_p$ ) retain their incoming energy. Viewed in the ISM rest system, they have, for large  $\gamma$ , a flat spectrum extending up to  $E \simeq 2\gamma^2 m c^2$  [this is recognizable as the

forward, massive-particle,  $z = 0$ , analog of Eq. (12)]. Thus, a moving CB is a gorgeous *Lorentz-boost accelerator*: the particles it elastically scatters reach up to, for  $\gamma = \gamma_0 = (1 \text{ to } 1.5) \times 10^3$ , an  $A$ -dependent **knee** energy  $E_{\text{knee}}(A) \sim (2 \text{ to } 4) \times 10^{15} \text{ A eV}$ . If this trivial process is the main accelerator of CRs, there must be a feature in the CR spectra: endpoints at  $E_{\text{knee}}(A)$ . The arrows in fig. 3 show that the H and He data are compatible with this prediction. So does the second knee of fig. 1a, the predicted Fe knee. The CR flux above the H knee, to which we shall return, is  $\sim 10^{-15}$  of the total.

### 11.2 The spectra below the knee

The ‘elastic’ scattering we just described is dominant below the knees. To compute the resulting spectrum, we assume that the ISM particles a CB intercepts, trapped in its magnetic mesh, reexit it by diffusion, isotropically in the CB’s system, and with the same ‘confinement’ law, Eq. (1), as in the Galaxy (the opposite assumption, that they are immediately elastically scattered, yields a slightly different spectral index). The CB deceleration law is Eq. (9), its radius evolves as in Eq. (8). A modest amount of algebra gives a simple result (DD06), which, for  $\gamma > 2$  and to a good approximation, reads<sup>2</sup>:

$$\frac{dF_{\text{elast}}}{d\gamma_{\text{CR}}} \propto n_A \left( \frac{A}{Z} \right)^{\beta_{\text{conf}}} \int_1^{\gamma_0} \frac{d\gamma}{\gamma^{7/3}} \int_{\max[\gamma, \gamma_{\text{CR}}/(2\gamma)]}^{\min[\gamma_0, 2\gamma\gamma_{\text{CR}}]} \frac{d\gamma_{\text{co}}}{\gamma_{\text{co}}^4}, \quad (15)$$

where  $\gamma_{\text{CR}}$  is the CR’s LF, and  $\beta_{\text{conf}}$  is the same confinement index as in Eq. (1). The flux  $dF_{\text{elast}}/d\gamma_{\text{CR}}$  depends on the priors  $n_A$ ,  $\beta_{\text{conf}}$ , and  $\gamma_0$ , but not on any parameter specific to the mechanism of CR acceleration. But for the normalization, this flux is  $A$ -independent. In the large range in which it is roughly a power law,  $dF_{\text{elast}}/d\gamma_{\text{CR}} \propto [\gamma_{\text{CR}}]^{-\beta_{\text{CR}}}$ , with  $\beta_{\text{CR}} = 13/6 \approx 2.17$ .

The H, He and Fe fluxes of fig. 3 are given by Eq. (15), modified by the Galactic confinement  $\tau$ -dependence of Eq. (1), with  $\beta_{\text{conf}} = 0.6$ . The fastest-dropping curve in fig. 3a corresponds to a fixed  $\gamma_0$ . The other two curves are for the  $\gamma_0$  distribution of fig. 13a, and one twice as wide. The low-energy data of fig. 1b are also described by Eq. (15), whose shape in this region (the ‘hip’, also visible in fig. 3c for Fe) is insensitive to  $\gamma_0$  and, thus, parameter-independent.

### 11.3 The relative abundances

It is customary to discuss the composition of CRs at a fixed energy  $E_A = 1 \text{ TeV}$ . This energy is relativistic, below the corresponding knees for all  $A$ , and in the domain wherein the fluxes are dominantly elastic and well approximated

---

<sup>2</sup>I am keeping factors of  $A/Z$  for kicks. Numerically, they are irrelevant: the theory and data are not so precise, and  $(A/Z)^{0.6}$  is 1 for H, 1.6 for Fe.

by a power law of index  $\beta_{\text{th}} = \beta_{\text{elast}} + \beta_{\text{conf}} \simeq 2.77$ . Expressed in terms of energy ( $E_A \propto A \gamma$ ), and modified by confinement as in Eq. (1), Eq. (15) becomes:

$$dF_{\text{obs}}/dE_A \propto \bar{n}_A A^{\beta_{\text{th}}-1} E_A^{-\beta_{\text{th}}}, \quad X_{\text{CR}}(A) = (\bar{n}_A/\bar{n}_p) A^{1.77}, \quad (16)$$

with  $\bar{n}_A$  an average ISM abundance and  $X_{\text{CR}}(A)$  the CR abundances relative to H, at fixed  $E$ . The results, for input  $\bar{n}_A$ 's in the 'superbubbles' wherein most SNe occur, are shown in Fig. 2b. In these regions, the abundances are a factor  $\sim 3$  more 'metallic' than solar (a 'metal' is anything with  $Z > 2$ ). Eq. (16) snugly reproduces the large enhancements of the heavy-CR relative abundances, in comparison with solar or superbubble abundances (e.g.  $A^{1.77} = 1242$  for Fe). The essence of this result is deceptively simple: in the kinematics of the collision of a heavy object (a CB) and a light one (the ISM nucleus), their mass ratio ( $N_{\text{B}}/A \sim \infty!$ ) is irrelevant.

#### 11.4 Above the knees

We discussed around Eq. (7) the generation of turbulently-moving magnetic fields (MFs) in the merger of two plasmas. Charged particles interacting with these fields tend to gain energy: a relativistic-injection, 'Fermi' acceleration process, for which numerical analyses<sup>18)</sup> result in a spectrum  $dN/dE \propto E^{-2.2}$ ,  $p \sim 2.2$ . For the ISM/CB merger, we (DD04) approximate the spectrum of particles accelerated within a CB, in its rest system, as:

$$dN/d\gamma_A \propto \gamma_A^{-2.2} \Theta(\gamma_A - \gamma) \Theta[\gamma_{\text{max}}(\gamma) - \gamma_A], \quad \gamma_{\text{max}} \simeq 10^5 \gamma_0^{2/3} (Z/A) \gamma^{1/3}, \quad (17)$$

The first  $\Theta$  function reflects the fact that it is much more likely for the light particles to gain than to lose energy in their elastic collisions with the heavy 'particles' (the CB's turbulent MF domains). The second  $\Theta$  is the Larmor cutoff implied by the finite radius and MF of a CB, with a numerical value given for the typical adopted parameters. But for the small dependence of  $\gamma_{\text{max}}$  on the nuclear identity (the factor  $Z/A$ ), the spectrum of Eq. (17) is universal. Boosted by the CB's motion, an accelerated and re-emitted particle may reach a Larmor-limited  $\gamma_{\text{CR}}[\text{max}] = 2 \gamma \gamma_{\text{max}}$ , a bit larger, for  $\gamma = \gamma_0 \sim 1.5 \times 10^3$ , than the corresponding GZK cutoffs. Our model has a *single source*, CBs, for the acceleration of CRs from the lowest to the largest observed energies.

The calculation of the 'elastic' spectrum of Eq. (15) was done for the bulk of the ISM particles entering a CB, assuming that they were not significantly Fermi-accelerated, but kept their incoming energy, i.e.  $dN/d\gamma_A \propto \delta(\gamma_A - \gamma)$ . The 'inelastic' spectrum, with  $dN/d\gamma_A$  as in Eq. (15), yields an equally simple result. The two  $E^2$ -weighed spectra are shown (for H) in fig. 14. The inelastic contribution is a tiny fraction of the total, and is negligible below the knee, a point at which we may compare the ratio of fluxes,  $f$ , the only parameter freely

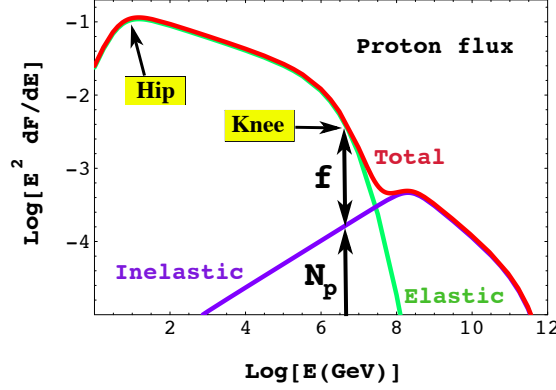


Figure 14: Contributions to the  $E^2$ -weighed proton source spectrum.

fit to the CR data. The boost of ISM particles by a CB and their acceleration within it are mass-independent, so that the ratio  $f$  is universal.

The  $E^3$ -weighed *source* spectra for the main elements are shown in fig. 15a. They are very different from the *observed* spectra of fig. 15b, for many reasons. Below the ankle(s) the slopes differ due to Galactic confinement, see Eq. (1). Above the ankles the flux from Galactic sources is strongly suppressed: we would see their straight-moving CRs only for CB jets pointing to us. The CRs above the ankle are mainly extragalactic in origin, and they also cross the Galaxy just once. Extragalactic CRs of  $A > 1$  are efficiently photo-dissociated by the cosmic infrared light. Extragalactic CRs are GZK-cutoff. All this can be modeled with patience and fair confidence. Below the ankle extragalactic CRs may have to fight the CR ‘wind’ of our Galaxy, analogous to that of the Sun. We have covered our lack of information on this subject by choosing two extreme possibilities (DD06), resulting in the two curves of figs. 1a and 4a,b.

In fig. 4b I have converted the results of fig. 15b into a prediction for  $\langle \text{Ln } A(E) \rangle$ . The flux at the second knee is dominated by Galactic Fe at its knee. Thereafter this flux decreases abruptly to let extragalactic H dominate all the way from the ankle to the nominal position of the proton’s GZK cutoff. Above that point the high-energy tail of Galactic Fe may dominate again.

### 11.5 The CR luminosity, and the overall normalization of the CR flux

The rate of core-collapse SNe in our Galaxy is  $R_{\text{SN}} \sim 2$  per century. In the CB model, we contend that  $\sim 50\%$  of the energy of CRs is transferred to the magnetic fields *they* generate<sup>25)</sup>. If all core-collapse SNe emit CBs, the Galactic CR luminosity should be  $L_{\text{CR}} \sim R_{\text{SN}} E_{\text{jets}}/2 \sim 4.7 \times 10^{41} \text{ erg s}^{-1}$ , with  $E_{\text{jets}}$  as in Eq. (5). This is 3 times larger than the rhs of Eq. (2). The ‘discrepancy’ is

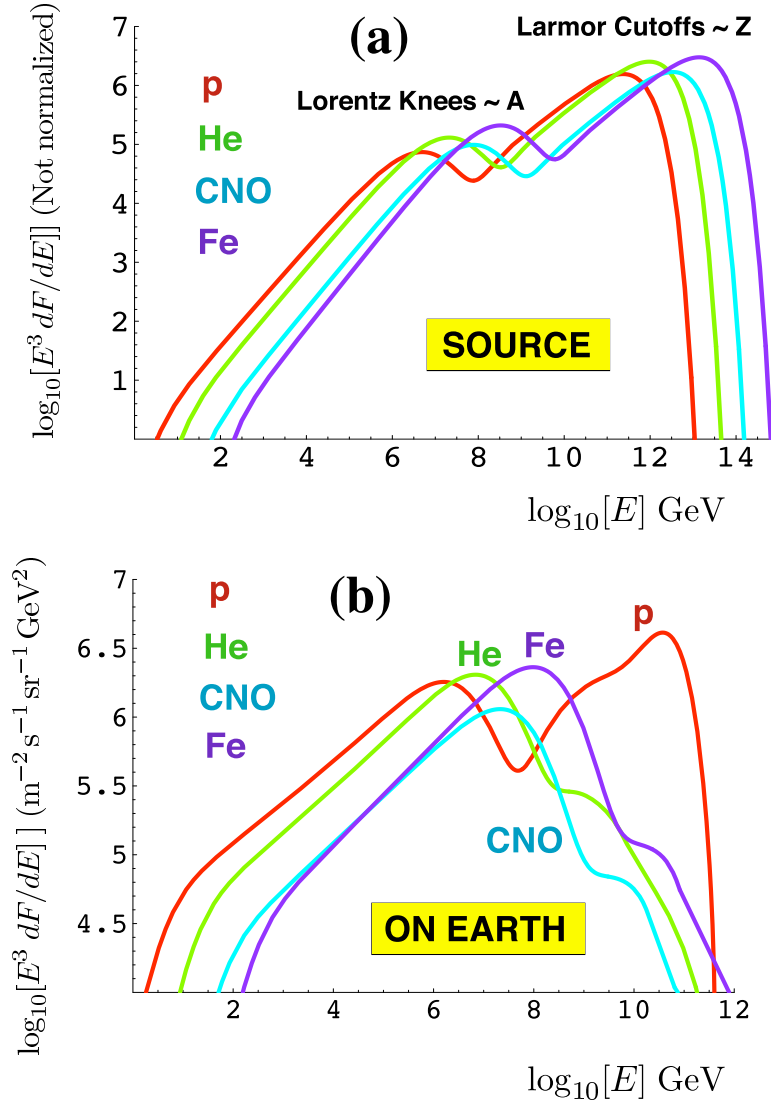


Figure 15: Predicted spectra for the abundant elements and groups. The vertical scales are  $E^3 dF/dE$ . (a): The source spectra, with a common arbitrary normalization. (b): The normalized CR spectra at the location of the Earth. Notice that the horizontal and vertical scales are different in (a) and (b).

not worrisome. A smaller fraction of SNe may generate high- $\gamma_0$  CBs. The rhs of Eq. (2) is for ‘standard’ CRs, but the confinement volume and time of the CB model are non-standard by factors of  $\sim 10$ . All inputs are fairly uncertain.

The calculation of the flux above the ankle is lengthy but straightforward. But for the GZK effect, its shape is that of the source H flux, since protons at that energy should escape other galaxies directly, and enter ours unhindered. Its normalization per SN is fixed. The SN rate per unit volume is measured in the local Universe. The overall flux is the result of the integration over redshift of the flux from past SNe. The integrand must be properly red-shifted and weighed with the star-formation rate as a function of  $z$  (SN progenitors have short lives on Hubble-time scales). The integration in  $z$  is an integration over look-back time, as opposed to distance, since CRs do not travel straight. The error in the result is hard to estimate, its central value is within a factor of 2 of the observations (DD06). This explains the coincidence that the ankle is the escape energy of protons from the Galaxy *and* the place where the extragalactic flux –not enhanced by confinement and thus less steep– begins to dominate.

#### 11.6 CR diffusion, CR electrons, and the $\gamma$ background radiation

In the standard paradigm CRs are accelerated by the nonrelativistic ejecta of SNe. SNe occur mainly in the central realms of the Galaxy, so that CRs must diffuse to arrive to our location. A directional asymmetry is predicted, and not observed <sup>26)</sup>. For CR electrons the problem is even more severe: their cooling time in the Galaxy’s light, and magnetic fields, is so short that they should have lost all their energy on their way here.

Our source distribution is totally non-standard, CBs generate CRs all along their many-kpc-long trajectories, see Eq. (9) and fig. 12c. Depending on the ISM density profile they encounter, CBs may travel for up to tens of kpc before they become nonrelativistic. It takes some  $6 \times 10^4$  years to travel 20 kpc at  $v \sim c$ . If a Galactic SN occurs every 50 years, and emits an average of 10 CBs, there are currently several thousand CBs in the Galaxy and its halo. This is a very diffuse CR source, satisfactory in view of the previous paragraph. We have not yet studied the CR source-distribution and diffusion in detail.

Below their knee at  $2\gamma_0^2 m_e c^2 \sim 2.3$  TeV, the source spectrum of CB-accelerated electrons has the same index as that of nuclei:  $dN/dE_e \propto E^{-\beta_{\text{CR}}}$ ,  $\beta_{\text{CR}} \approx 2.17$ . The predicted spectrum <sup>27)</sup>, steepened by radiative energy losses, has an index  $\beta_e = \beta_{\text{CR}} + 1 \approx 3.17$ . Its observed slope <sup>28)</sup> is  $3.2 \pm 0.1$  above  $E_e \sim 10$  GeV, an energy below which other losses should dominate (DD06).

The Gamma Background Radiation (GBR), measured by EGRET from a few MeV to  $\sim 10^5$  MeV, was argued to be dominantly of cosmological origin, in directions above the disk of the Galaxy and away from its bulge <sup>29)</sup>. A more careful analysis reveals a significant correlation of its intensity with our

position relative to the Galactic centre <sup>27)</sup>. The CB-model reproduces this correlation, provided a good fraction of the GBR is generated by CR electrons at high galactic latitudes, as they cool radiatively by the very same process that steepens their spectrum. The predicted index of the radiated GBR photons is  $\beta_\gamma = (\beta_e - 1)/2 = 2.08$ . The observed one <sup>29)</sup> is  $2.10 \pm 0.03$ .

## 12 If CBs are so pervasive, why are they not readily observed?

The answer is simple. The CBs of SNe are tiny astrophysical objects: their typical mass is half of the mass of Mercury. Their energy flux at all frequencies is  $\propto \delta^3$ , large only when their Lorentz factors are large. But then, the radiation is also extraordinarily collimated, it can only be seen nearly on-axis. Typically, observed SNe are too far to *photograph* their CBs with sufficient resolution.

Only in two SN explosions that took place close enough, the CBs were in practice observable. One case was SN1987A, located in the LMC, whose approaching and receding CBs were photographed, see fig. 6e,f. The other case was SN2003dh, associated with GRB030329, at  $z = 0.1685$ . In the CB model interpretation, its two approaching CBs were first ‘seen’, and fit, as the two-peak  $\gamma$ -ray light curve of fig. 5b and the two-shoulder AG of fig. 6a,b. This allowed us to estimate the time-varying angle of their superluminal motion in the sky <sup>17)</sup>. Two sources or ‘components’ were indeed clearly seen in radio observations at a certain date, coincident with an optical AG rebrightening. We claim that the data agree with our expectations<sup>3</sup>, including the predicted inter-CB separation <sup>17)</sup> of fig. 6d. The observers claimed the contrary, though the evidence for the weaker ‘second component’ is  $> 20\sigma$ . They report <sup>30)</sup> that this component is ‘not expected in the standard model’. The unpublished and no-doubt spectacular-discovery picture of the two superluminally moving sources would have been worth a thousand words... in support of the CB model.

## 13 Other CR sources

We have defended the simplistic view that CBs from SNe is all one needs to generate CRs at all energies. The recent data of Auger <sup>31)</sup> show a significant correlation between the arrival directions of ultra-high energy CRs (UHE-CRs) and Active Galactic Nuclei (AGNs) located within a distance of 75 Mpc

---

<sup>3</sup>The size of a CB is small enough to expect its radio image to scintillate, arguably more than observed <sup>30)</sup>. Admittedly, we only realized a posteriori that the ISM electrons a CB scatters, synchrotron-radiating in the ambient magnetic field, would significantly contribute at radio frequencies, somewhat blurring the CBs’ radio image <sup>17)</sup>.



( $z \sim 0.02$ ), comparable to the GZK ‘horizon’ at the observed energies,  $E > 56$  EeV. As the authors discuss, this does not mean that AGNs are the actual sources<sup>32)</sup>, for AGNs are themselves correlated with matter and with active regions of enhanced stellar birth and death. More work on correlations is no doubt in progress. A search for correlations with GRBs is less hopeful, for the fraction of them observed from within  $z \sim 0.02$  is negligible, and the observed ‘correlated’ CRs may have been bent by magnetic fields up to a few degrees, implying a possible delay of millenia between the arrival times of  $\gamma$ ’s and CRs.

Observations of AGNs are an ingredient of the ‘inspiration’ of the CB model, as we have discussed in connection with Pictor A, see fig. 11a,b. Naturally, we have estimated their contribution to the UHECR proton flux, concluding that they may constitute at most 1 to 10% of the flux generated by extragalactic SNe (DD04). The estimate is for the energy-integrated flux; in applying it to UHECRs we assumed the same energy dependence for the flux generated –by the same mechanisms– by the CBs of SNe and AGNs (a small difference of spectral index implies an enormous uncertainty). In a subsequent study<sup>33)</sup> of the CR electron flux, assumed to be in a fixed proportion to the proton flux, we used more recent inputs, and simplified and modified our upper limit to 40%. But we forgot<sup>4</sup> to extract the putative consequences for the AGN contribution to UHECR protons!

## 14 Discussion and conclusion

We do not have a solid understanding of accretion onto black holes or neutron stars. But such processes are observed to result in the ejection of relativistic and highly collimated jets. We assumed that a similar process takes place as a stellar core collapses, leading to a supernova event. We posited that the SN’s relativistic ejecta –two jets of cannonballs– are the sources of GRBs and CRs. The association between SNe and (long) GRBs is now established. We argued that the electrons in a CB, by inverse Compton scattering on the illuminated surroundings of the exploding star, generate the  $\gamma$  rays, X-rays, UV and optical light of the ‘prompt’ phase of a GRB. The ensuing results are the simplest and most predictive, they are a firm ‘theory’. In this paper I have, however, followed the historical development, in which the CB parameters were first extracted from the observations of the afterglow of GRBs. This involves a ‘model’, a set of arguable but simple hypothesis leading to the prediction of the properties of the AG –dominated by synchrotron radiation by the ISM electrons that a CB intercepts– as a function of frequency and time. In the historical order

---

<sup>4</sup>In these days of large experimental collaborations percolated by theorists, rumours herald publications. It might have been possible to turn this comment into a renewed<sup>32)</sup> timely ‘prediction’, prior to the Auger announcement.

the ‘prompt’ results for GRBs are predictions of the theory. Some results for Cosmic Rays –the ISM particles that CBs scatter in their journey– are also ‘theory’, others can be viewed as further tests of the ‘model’.

The results for GRB afterglows may be based on a simplified model, but they work with no exception all the way from radio to X-rays (DDD02,03). In particular, they describe correctly GRB 980425, located at a redshift two orders of magnitude closer than average. Its associated SN is the one we ‘transported’ to conclude –thanks to the reliability of our AG model– that core-collapse SNe generate long GRBs (DDD02). The X-ray light curve of GRB 980425 and a few others, with extremely scarce data, was described with the ‘canonical’ properties later observed in detail in many SWIFT-era GRBs. It is not recognized that the two CBs of GRB 030329 were seen, or that their separation in the sky was the predicted ‘hyper-luminal’ one. In view of the overall success of the CB model, this is a durable hurdle: GRBs so close and luminous are very rare.

The accuracy of the predictions for the prompt phase of GRBs amazes even the CB-model’s proponents. The typical values and the correlations between the  $\gamma$ -ray prompt observables leave little doubt that the production mechanism is inverse Compton scattering on ‘ambient’ light of  $\sim 1$  eV energy. The approximate scaling law  $E dN_\gamma/dEdt \propto F(E t^2)$  –spectacularly confirmed in the case of XRF 060218– demonstrates that the light is that of a ‘glory’: the early SN light scattered by the ‘windy’ pre-SN ejecta. A GRB spectrum that works even better <sup>34)</sup> than the phenomenological ‘Band’ expression is also predicted. The flux and its spectral evolution during the prompt and rapid-decline phases are the expected ones, as we tested in minute detail with SWIFT data.

In the internal-external fireball model of GRBs, highly relativistic thin conical shells of  $e^+e^-$  pairs, sprinkled with a finely tuned baryon ‘load’, collide with each other generating a shock that accelerates their constituents and creates magnetic fields. Each collision of two shells produces a GRB pulse by synchrotron radiation. The ensemble of shells collides with the ISM to produce the AG by the same mechanism. The energy available to produce the GRB pulse –as two shells moving in the *same* direction collide– is more than one order of magnitude smaller than that of the merged shells as they collide with the ISM at rest. The ratio of observed GRB and AG energies is more than one order of magnitude, but in the opposite direction. This ‘energy crisis’ in the comparison of bolometric prompt and AG fluences <sup>4)</sup> is not resolved. Moreover, the GRB spectrum cannot be accommodated on grounds of synchrotron radiation <sup>35)</sup>, the ‘standard’ prompt mechanism. The SWIFT-era observations also pose decisive problems to the standard model, whose microphysics <sup>36)</sup>, reliance on shocks <sup>37)</sup> and correlations based on the jet-opening angle <sup>38)</sup> have to be abandoned, according to the cited authors.

In spite of the above, the defenders of the fireball model are not discour-

aged. Their attitude towards the CB model, whose observational support is so remarkable, is not equally supportive. This may be due to cultural differences. Particle physicists believe that complex phenomena may have particularly simple explanations. They thrive on challenging their standard views. Doubting or abandoning a previous consensus in astrophysics is less easy.

The CB-model description of Cosmic Rays is also simplistic: there is only one source of (non-solar) CRs at all energies, and only one parameter to be fit. The model has a certain inevitability: if CBs with the properties deduced from GRB physics are a reality, what do they do as they scatter the particles of the interstellar medium? We have argued that they transmogrify them into CRs with all of their observed properties. The mechanism is entirely analogous to the ICS responsible for a GRB's prompt radiation. Suffice it to substitute the CB's electron, plus the ambient photon, by a moving-CB's inner magnetic field, plus an ambient nucleus or electron.

After a century of CR measurements, the CB-model results lack the glamour of predictions. Yet, the expectations for the knee energies, and for the relative abundances of CRs, are 'kinematical', simple, and verified. They constitute evidence, in my opinion, that the underlying model is basically correct. The prediction for the shape of the spectra: the low energy hips, the large energy stretch very well described by a power-law of (source) index  $\beta_s = 13/6$ , and the steepening at the knees, are also verified. The index  $\beta_s$  is measured well enough for the adequacy of the prediction to be sensitive to the details of the underlying model, such as the form of the function  $R(\gamma)$  in Eq. (8). I cannot claim that the fact that the prediction is right on the mark is much more than a consistency test, for the physics underlying this aspect of the problem may be terrifyingly complex. The same CR source –cannonballs from supernovae, this time extragalactic– satisfactorily describes the CR data above the ankle. Finally, the properties of CR electrons, and of the high-latitude Gamma 'Background' Radiation, are also correctly reproduced.

Most CR scholars agree with the 'standard' paradigm that the flux well below the knee is produced by the acceleration of the ISM in the frontal shocks of the nonrelativistic ejecta of SNe. In spite of recent observations of large magnetic fields <sup>39)</sup> in collisions of SN shells and molecular clouds, nobody has been able to argue convincingly that this process can accelerate particles up to the (modest) energy of the knee, *and* to show that the number and efficiency of the putative sources suffices to generate the observed CR luminosity (to my satisfaction, I add, to make these statements indisputable). From this point on, there is no 'standard' consensus on the origin of CRs, e.g., of the highest-energy ones. In this sense, the CB model is regarded as yet another model, which it is. After all, we are only saying that CRs are accelerated by the jetted relativistic ejecta of SNe, as opposed to the quasi-spherical, non-relativistic ones. Yet, the CB model is also rejected by the CR experts, sometimes even in print <sup>1)</sup>,

though it survives the critique <sup>40)</sup>. But, concerning CRs, the model does not trigger the same indignant wrath as in the GRB realm.

I have shown that the problem of GRBs is convincingly –i.e. predictively– solved and that, on the same simple basis, all properties of CRs can be easily derived. Only an overwhelmed minority recognizes these facts, in contradiction with Popper’s and Ockham’s teachings. I would conclude with a dictum attributed to Lev Landau: *‘In astrophysics, theories never die, only people do.’*

### Acknowledgement

I thank Shlomo Dado, Arnon Dar and Rainer Plaga for our collaboration.

### References

1. A.M. Hillas, arXiv:astro-ph/0607109
2. J.R. Hoerandel, arXiv:astro-ph/0702370v2
3. P. Meszaros, arXiv:astro-ph/0605208
4. T. Piran, Rev. Mod. Phys. **76**, 1143 (2004); Phys. Rep. **333**, 529 (2000).
5. S. Dado, A. Dar & A. De Rújula, Astron. & Astrophys. **388**, 1079 (2002).
6. S. Dado, A. Dar & A. De Rújula, Astron. & Astrophys. **401**, 243 (2003).
7. A. Dar & A. De Rújula, Phys. Reps. **405**, 203, (2004).
8. A. Dar & A. De Rújula, arXiv:astro-ph/0606199
9. S. Dado, A. Dar & A. De Rújula, arXiv:0706.0080
10. A. Dar & A. De Rújula, Astroph. J. **547**, L33, (2001).
11. S. Dado, A. Dar & A. De Rújula, Astroph. J. **594**, L89, (2003).
12. P. Nisenson & C. Papaliolios, Astrophys. J. **518**, L29, (1999).
13. E. Maiorano *et al.* Astron. & Astroph. **438**, 821 (2005).
14. S. Campana, et al. Nature, **442**, 1008 (2006).
15. A. Dar & A. De Rújula, arXiv:astro-ph/0008474
16. A. De Rújula, Phys. Lett. **B193**, 514 (1987).
17. S. Dado, A. Dar & A. De Rújula, arXiv:astro-ph/0402374, 0406325
18. J.K. Frederiksen *et al.*, Astroph. J. **608**, L13 (2004); astro-ph/0303360

19. N. J. Shaviv & A. Dar, *Astroph. J.* **447**, 863 (1995).
20. A. Dar & A. De Rújula, arXiv:astro-ph/0012227
21. S. Dado, A. Dar & A. De Rújula, *Astroph. J.* **663**, 400, (2007).
22. S. Dado, A. Dar & A. De Rújula, arXiv:astro-ph/0701294
23. S. Dado, A. Dar & A. De Rújula, arXiv:0709.4307
24. S. Dado, A. Dar & A. De Rújula, to be published.
25. A. Dar & A. De Rújula, *Phys. Rev.* **D72**, 123002, (2005).
26. R. Plaga, arXiv:astro-ph/0111555
27. A. Dar & A. De Rújula, *Mon. Not. Roy. Astron. Soc.* **323**, 391, (2001).
28. M. Aguilar *et al.*, *Phys. Rep.* **366**, 331 (2002).
29. P. Sreekumar *et al.*, *Astrophys. J.* **494**, 523 (1998).
30. G.B. Taylor *et al.* *Astrophys. J.* **609**, L1, (2004).
31. The Pierre Auger collaboration, *Science* **318**, 938 (2007).
32. V.L. Ginzburg & S.I. Syrovatskii, *The origin of Cosmic Rays* (Pergamon, Oxford, 1964).
33. S. Dado, A. Dar & A. De Rújula Nuc, *Phys. Proc. Suppl.* **B165**, 103 (2007)
34. C. Wigger *et al.* arXiv:0710.2858
35. G. Ghisellini, A. Celotti, & D. Lazzati, *MNRAS* **316**, L5 (2000).
36. A. Panaitescu *et al.* *MNRAS* **369**, 2059 (2006).
37. P. Kumar *et al.* *MNRAS* **376**, L57, (2007).
38. G. Sato *et al.* *Astroph. J.* **657**, 359, (2007);  
D. N. Burrows & J. Racusin, arXiv:astro-ph/0702633
39. Y. Uchiyama *et al.* *Nature* **449**, 576, (2007).
40. S. Dado, A. Dar & A. De Rújula, arXiv:astro-ph/0611369